Radiative models for rapid blazar flares : a focus on time delays

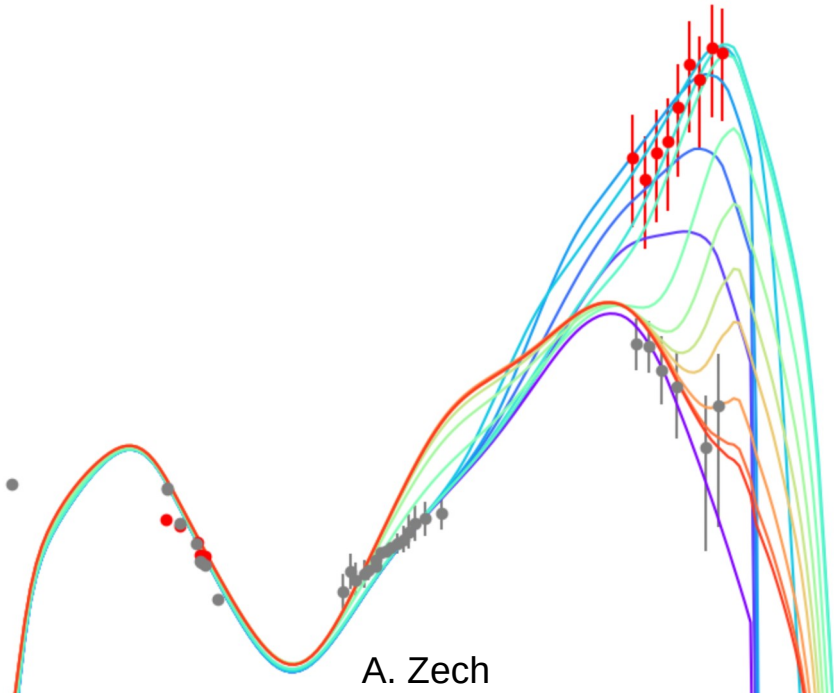

A. Zech

BridgeQG Workshop
Annecy, February 2026

LUX Observatoire de Paris | PSL

Modeling approaches for blazar variability

emission of different blazar types

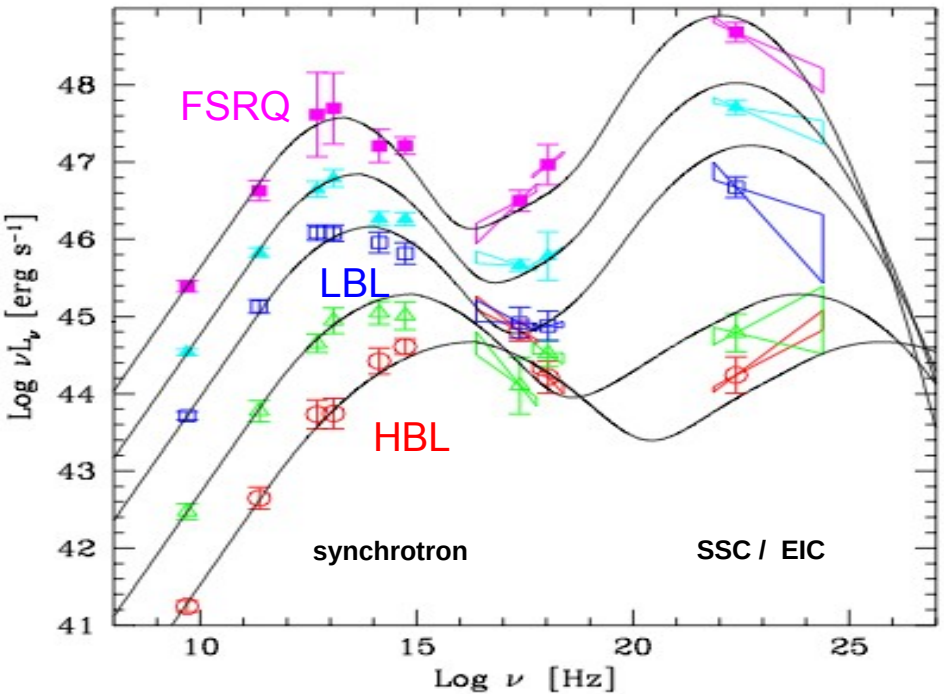

Donato et al. (2002), based on Fossati et al. (1998)

luminous **FSRQs** with low peak energies
↔ less luminous **BL Lac objects** with high peak energies

emission of different blazar types

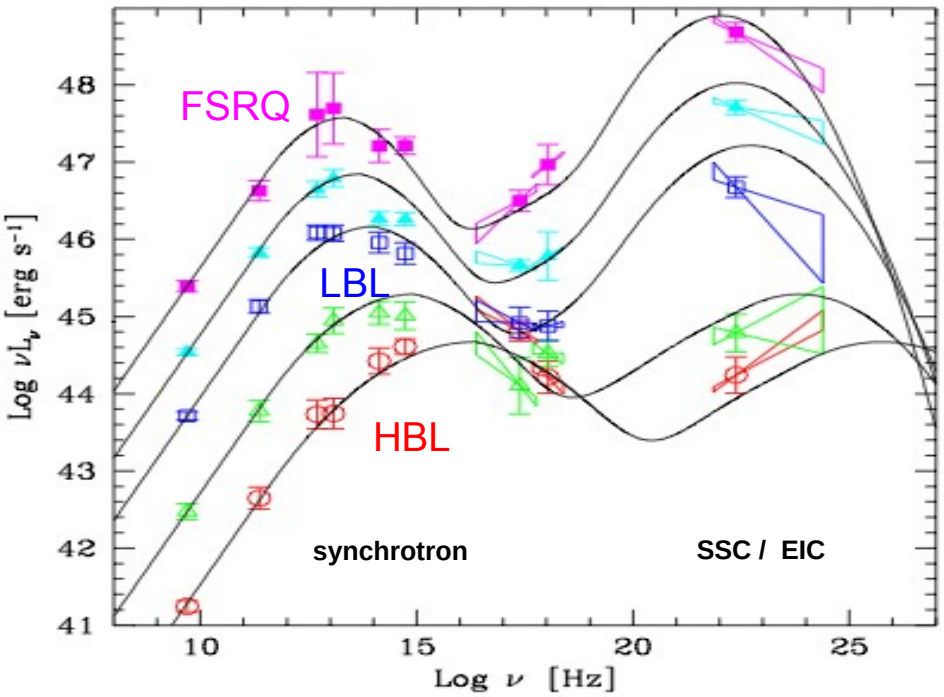

Donato et al. (2002), based on Fossati et al. (1998)

luminous **FSRQs** with low peak energies
↔ less luminous **BL Lac objects** with high peak energies

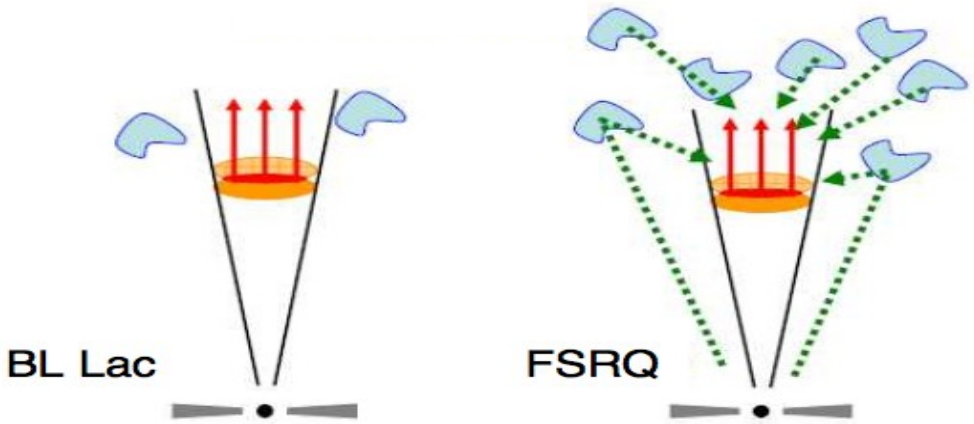

B. Lott, Cospar 02/10

- Disk, Broad Line Region, dust torus emit **weakly**

- leptonic models : γ-rays due to **Synchrotron Self Compton**

- hadronic models : **proton-synchrotron** dominates γ-rays ?

- Disk, Broad Line Region, dust torus emit **strongly**

- leptonic models: γ-rays mostly due to **External Inverse Compton**

- hadronic models : **proton-induced cascades** dominate γ-rays ?

flares : macroscopic vs. microscopic variations

variation of the macroscopic parameters of the emission region

- change in size of emission region R (expansion, contraction) or density

- change in magnetic field B or external radiation field

- change in Doppler beaming (Lorentz factor, viewing angle)

flares : macroscopic vs. microscopic variations

variation of the macroscopic parameters of the emission region

- change in size of emission region R (expansion, contraction) or density

- change in magnetic field B or external radiation field

- change in Doppler beaming (Lorentz factor, viewing angle)

variation in the energy distribution of the emitting particles

- particle injection (pre-accelerated particle distribution)

- particle acceleration (shock, turbulence, magnetic reconnection...)

2 complementary approaches : modeling stochastic variability patterns vs. individual flares

particle acceleration in jets

Possibly there is no single mechanism at play, but several mechanisms contribute in different regions of the jet.

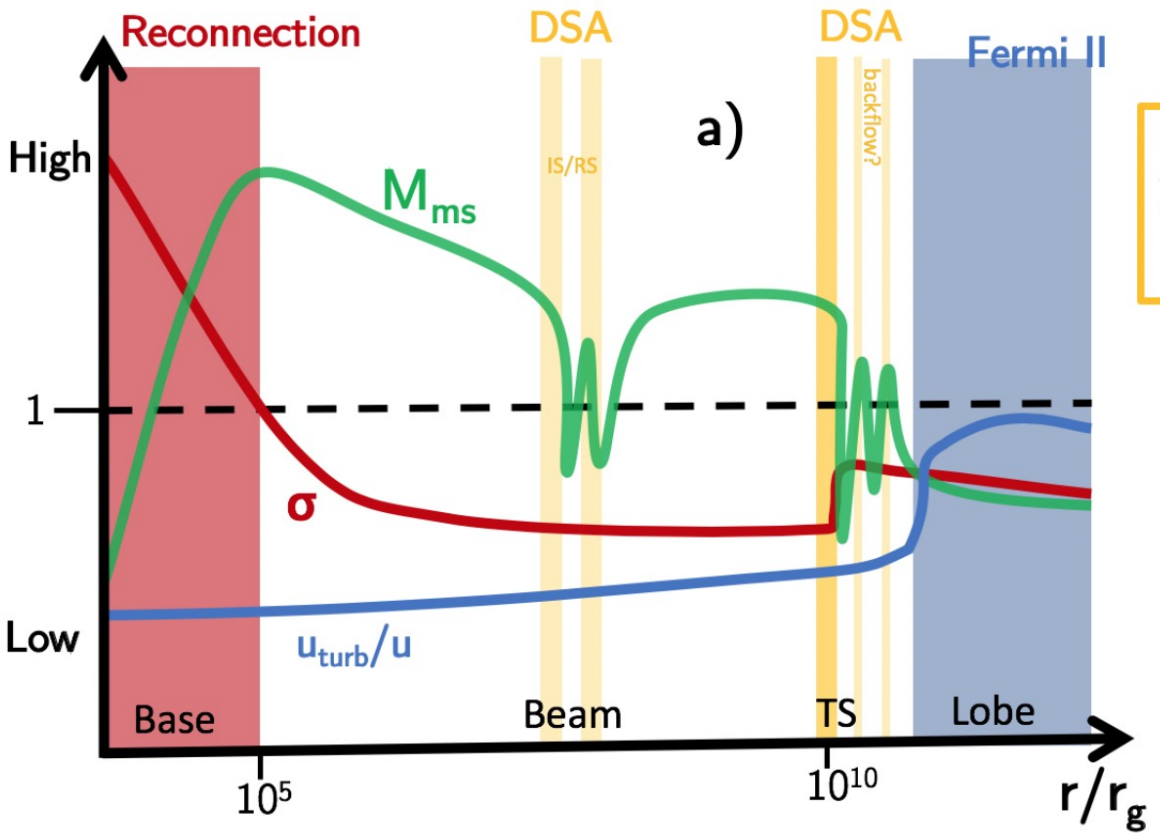

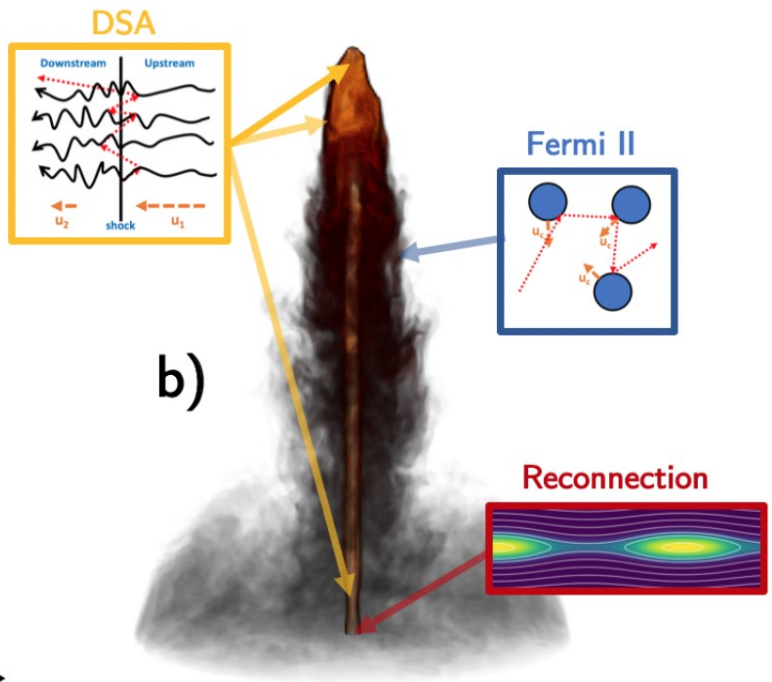

Matthews, Bell, Blundell 2020

Single-zone models : particle injection / acceleration

(here applied to BL Lacs)

particle evolution through injection or acceleration

- a single zone is responsible for the low-state and flare emission
- flares arise from a variation of the electron distribution in the zone
- particle distribution described by Fokker-Planck equation (e.g. EMBLEM code) :

Cooling terms — Acceleration terms

$$\frac{\partial N_e(\gamma,t)}{\partial t} = \frac{\partial}{\partial \gamma}\left[\left(b_c(\gamma,t)\gamma^2 + \frac{1}{t_{ad}}\gamma - a(t)\gamma - \frac{2}{\gamma}D_{F_{II}}(\gamma,t)\right)N_e(\gamma,t)\right] + \frac{\partial}{\partial \gamma}\left(D_{F_{II}}(\gamma,t)\frac{\partial N_e(\gamma,t)}{\partial \gamma}\right) - N_e(\gamma,t)\left(\frac{1}{t_{esc}} + \frac{3}{t_{ad}}\right) + \dot{Q}_{inj}(\gamma,t)$$

Injection term

Cooling

- Synchrotron and Inverse Compton: $b_c(\gamma,t) = \frac{4\sigma_T(u_B + u_{rad})}{3 m_e c}$
- Adiabatic expansion: $t_{ad}(t) = \frac{R(t)}{\beta_{exp} c}$

$\Rightarrow t_{cool} \propto 1/\gamma$

Acceleration

- Fermi I: $a = 1/t_{shock}$, $\dot{Q}(\gamma,t)$
- Fermi II: $D_{F_{II}}(\gamma,t) = \frac{p^2}{t_{F_{II}}}$

e.g. Fermi-I acceleration

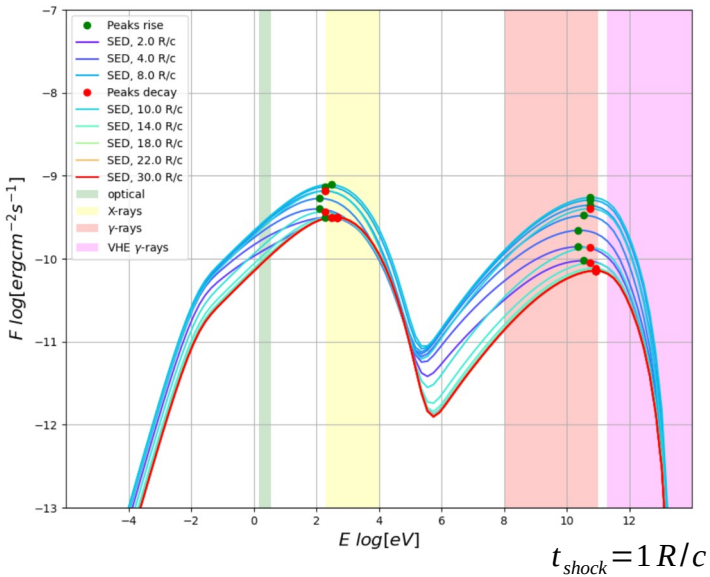

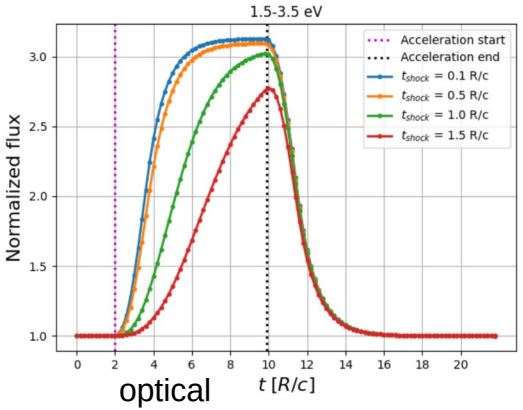

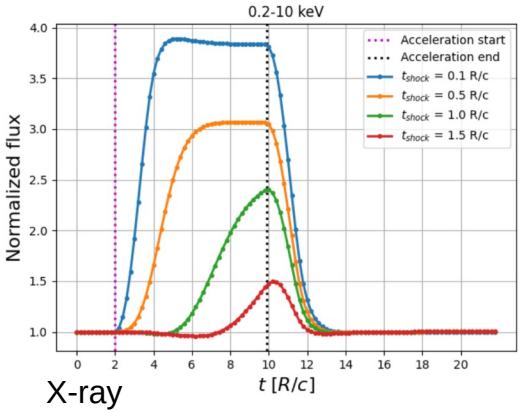

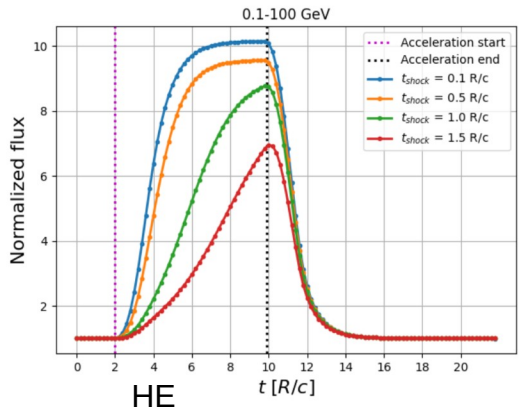

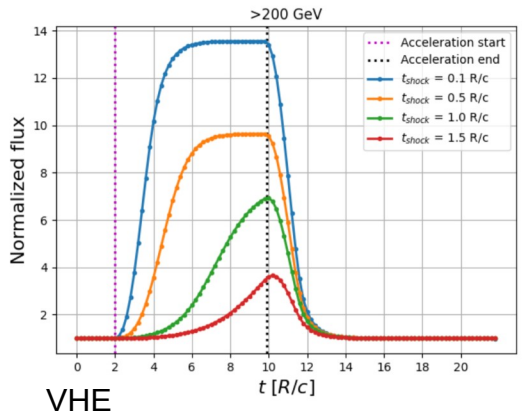

- shift of peaks during flare

- flare **onset** shifts between energy bands

- occurrence of a plateau
  (= high steady-state) only for very rapid t_{shock}

comparison with a 2013 flare of Mrk 421

- one single zone is not sufficient to describe the MWL behaviour
→ addition of a **baseline flux** to model the unknown continuum flux below the flare

- for this simplified application, the injection scenario (= very efficient Fermi-I acceleration) provides the best representation of the high-energy data

- **Time delays** :

Injection : early peak in X-rays due to IC cooling

Fermi I re-acceleration : earlier peak in VHE due to shift in target photon flux

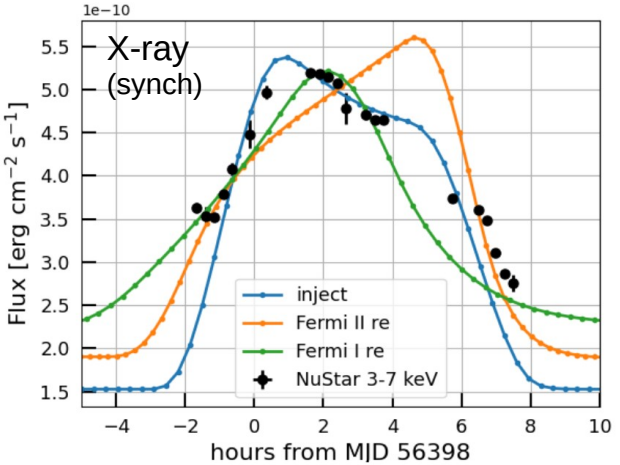

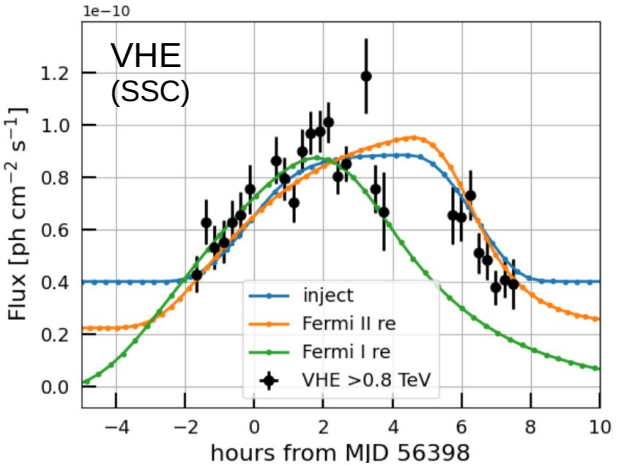

Thevenet, AZ, Dmytriiev, Boisson, accepted A&A

blob moving through turbulent jet region

In this model using several zones, the continuous low-state emission from Mrk 421 is connected with a flare in Feb. 2010 :

- low state is modelled with a continuous injection (+ cooling, escape) of electrons accelerated on a bow shock

- the hard flare spectrum requires additional Fermi II acceleration from a turbulent emission region surrounding the blob as it passes through an inhomogeneous region inside the jet.

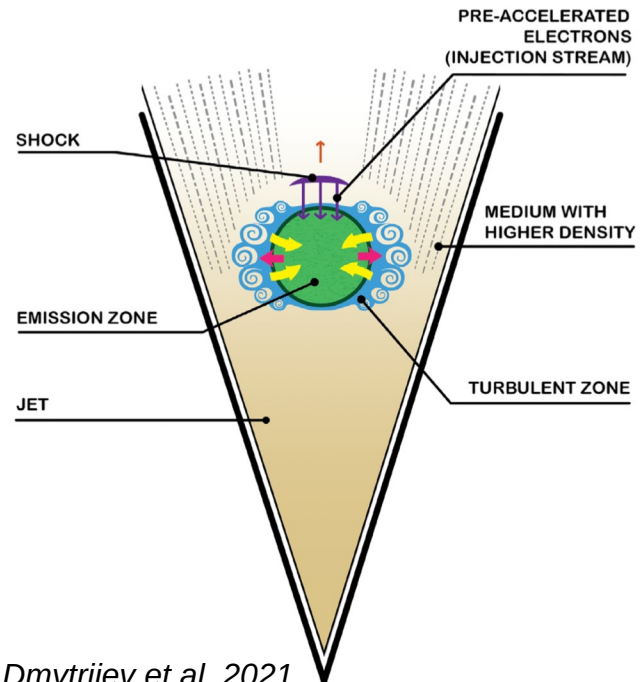

A. Dmytriiev et al. 2021

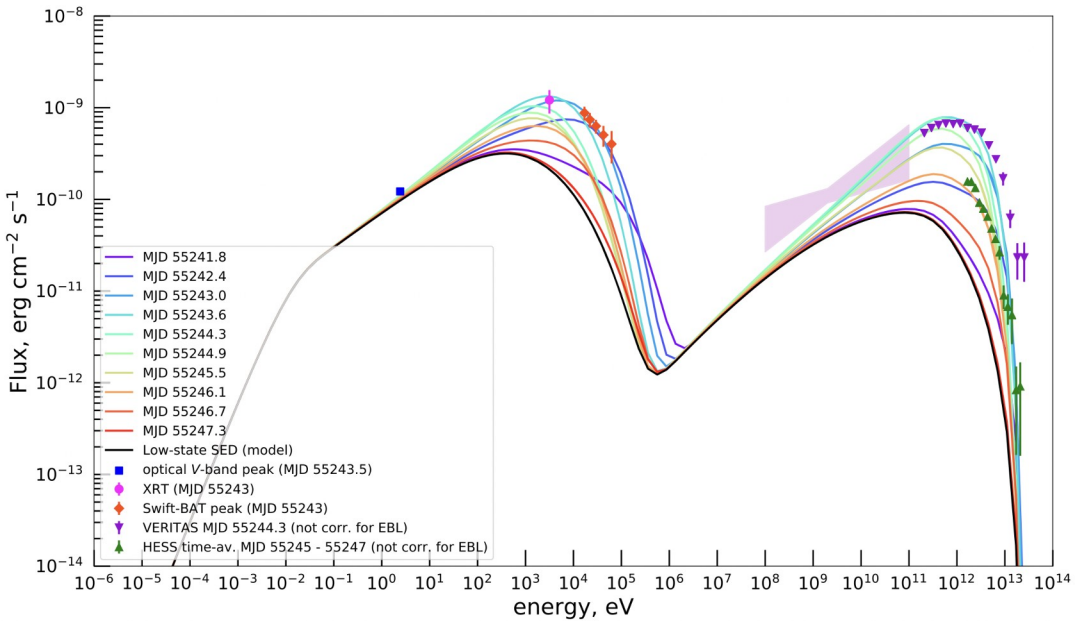

Broad-band emission from Mrk 421 during low state and flare + model curves.

blob moving through turbulent jet region

Time delays ?

HE band “synchronised” with **optical** band :
IC emission off optical photons

X-ray bands peak earlier than optical :
synchrotron emission from high-energy electrons with short cooling times

VHE bands peak a bit earlier than optical :
IC emission off higher energy photons

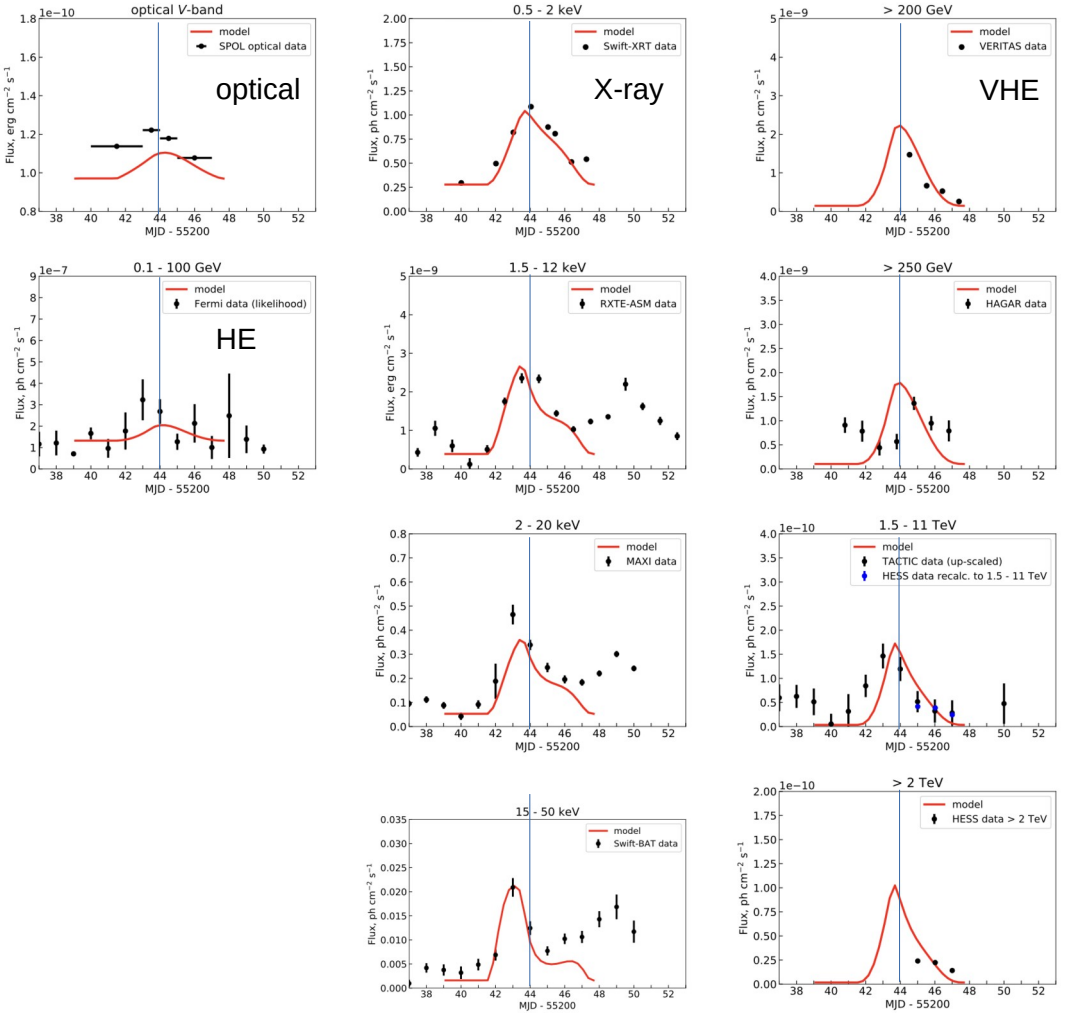

Single-zone models : propagation through photon fields

(application to FSRQs)

modeling the photon fields in a FSRQ

e.g. EMBLEM code

- External Compton emission on photon fields from accretion disk, corona, Broad Line Region, dust torus

- In many scenarios, the **BLR** has the most significant contribution (emission region at sub-pc scales) :

  -- photons from a spectrum of emission lines

  -- BLR modeled as a spherical shell with inner radius $R_{BLR} \sim 3 \times 10^{17}$ cm (0.1 pc)

  -- For distance d > R_{BLR}, the energy density decreases as :

$$U'(\epsilon', d) = \frac{L'_{BLR}(\epsilon')\Gamma^2_{blob}}{3\pi R^2_{BLR} c\left(1+\left(d/R_{BLR}\right)^{\beta_{BLR}}\right)}$$

  (Hayashida et al 2012)

  -- γ-γ absorption following *Böttcher & Els (2016)*

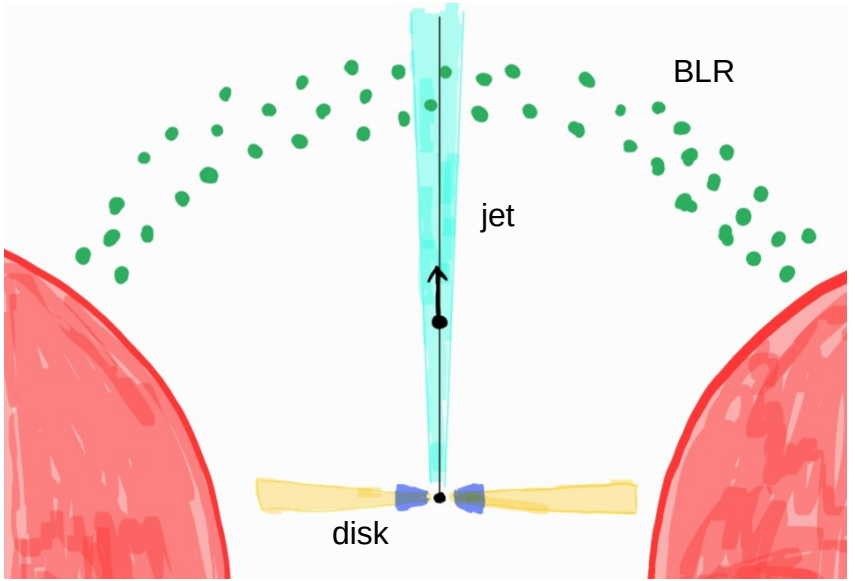

accelerating blob model

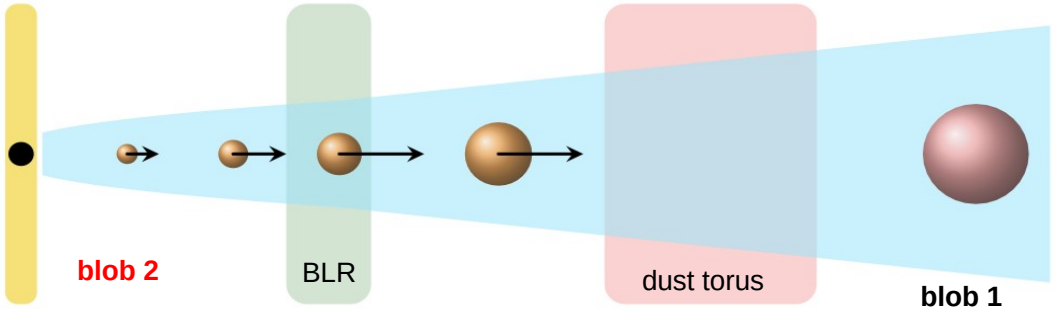

Le Bihan, Dmytriiev, AZ, 2025

low-state emission from a stationary emission region, e.g. recollimation shock ("**blob 1**")

flare is caused by an accelerating, expanding emission region ("**blob 2**")

→ acceleration through differential collimation up to ~ BLR

- for $d < R_{BLR}$, as blob 2 accelerates :

$$U' \propto d$$

- for $d > d_{max}$, as blob 2 advances at constant velocity :

$$U' \propto d^{-\beta_{BLR}}$$

- particle spectrum from injection of a steep power-law + cooling (incl. adiabatic) + particle escape

accelerating blob model

Low-state SED from ‘blob 1’

Flare is caused by ‘blob 2’

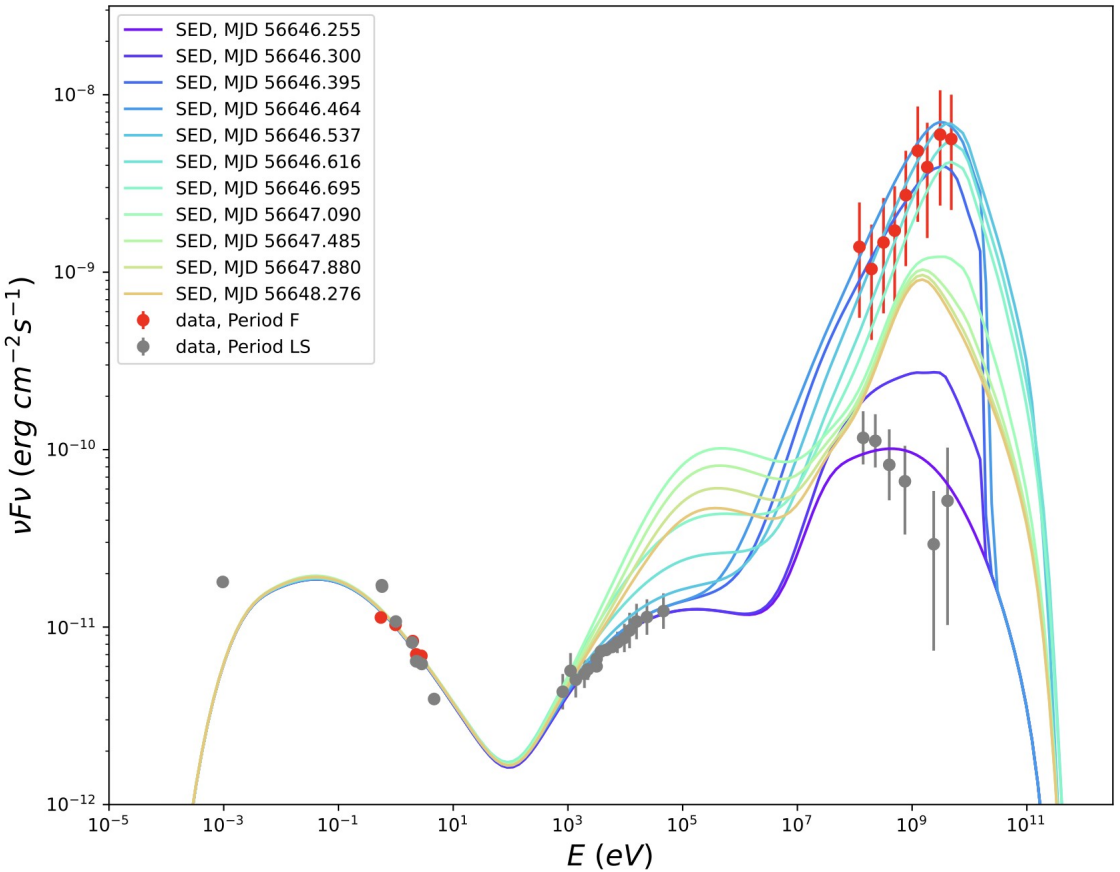

accelerating blob model

Time delays ?

VHE band : delayed wrt HE band due to γγ pair production on the BLR photons

X-ray band : delayed wrt HE band due to a slower onset of the synchrotron emission from the moving blob
Emission is dominated by EIC (HE, VHE) before SSC
flux (X-rays) rises above the low state flux

Optical band : no variation of the optical flux (by design)
The low-state flux always dominates in this band.

→ high-energy “orphan” flare

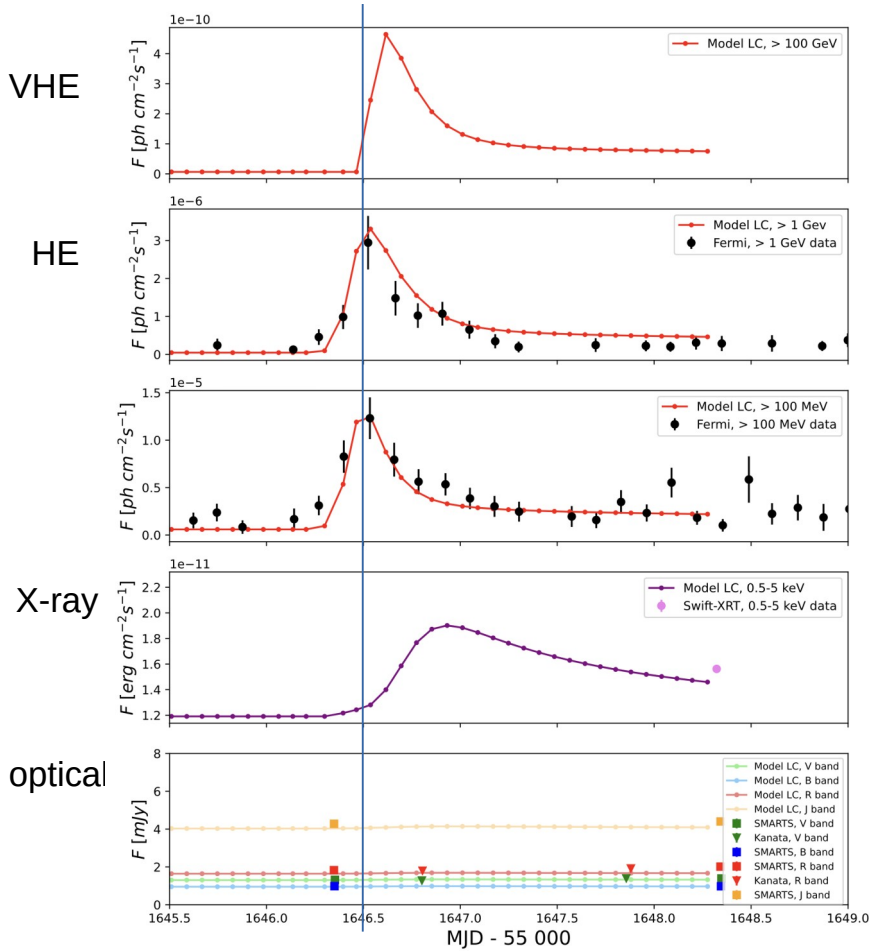

Multizone models

internal shocks

MUZORF model (multi-zone radiation feedback)

- emission of two relativistic plasma shells with different Lorentz factors into the jet

- faster inner shell catches up with slower outer shell → inelastic collisions produces **internal shock**
  → particle acceleration on the reverse and forward shock
  → emission of synchrotron and SSC radiation is followed across multiple cylindrical slices

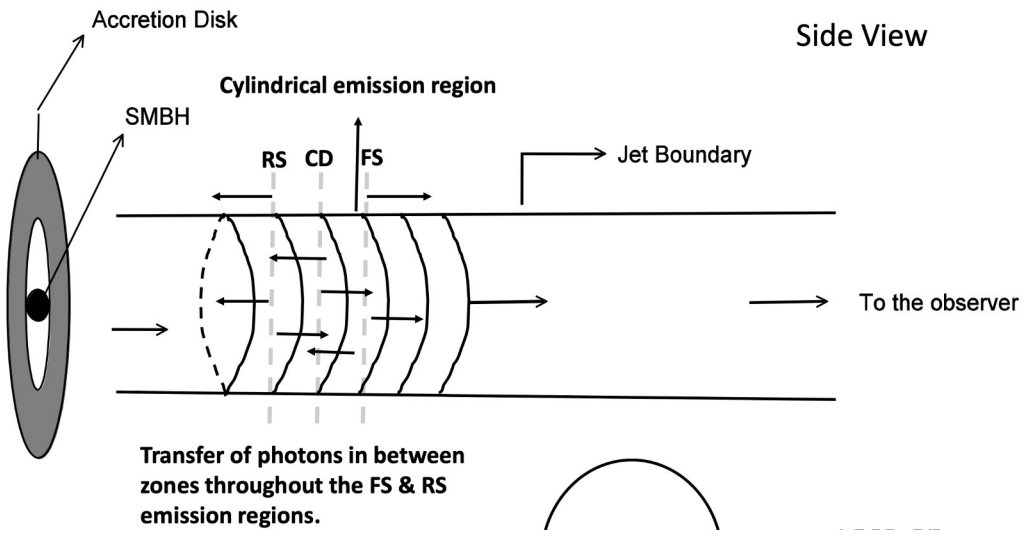

Joshi M. & Boettcher M., 2011, ApJ, 727, 21

internal shocks

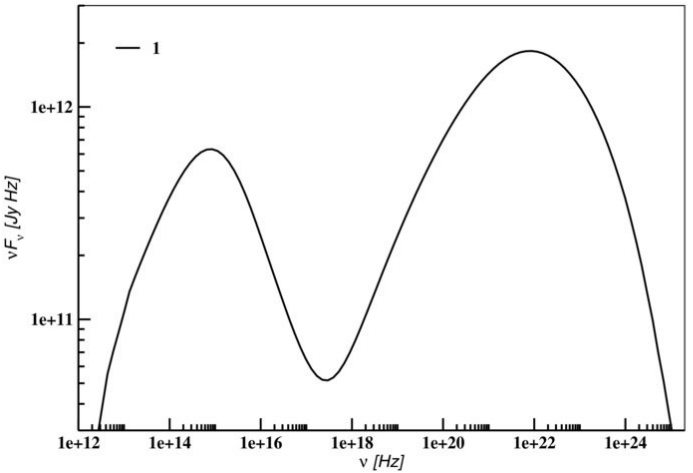

time-integrated SED

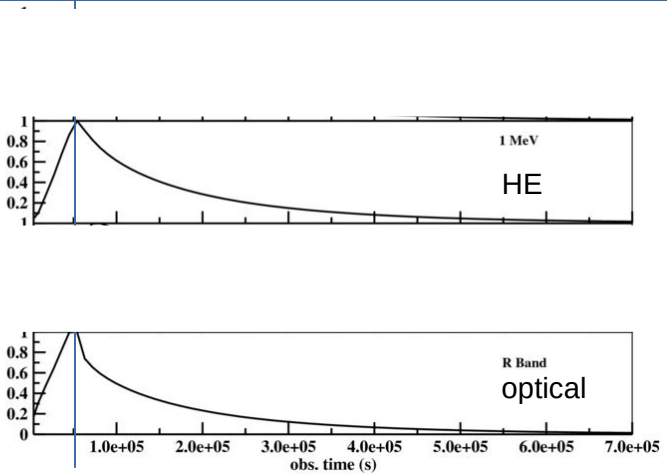

MWL light curves for a single collision.

optical flux : rise as long as the shocks are present in the emission region.
Then cooling dominates and the pulse begins to decline steadily.

HE photons : result of Compton up-scattering of optical photons off low-energy electrons → same peak as optical

internal shocks

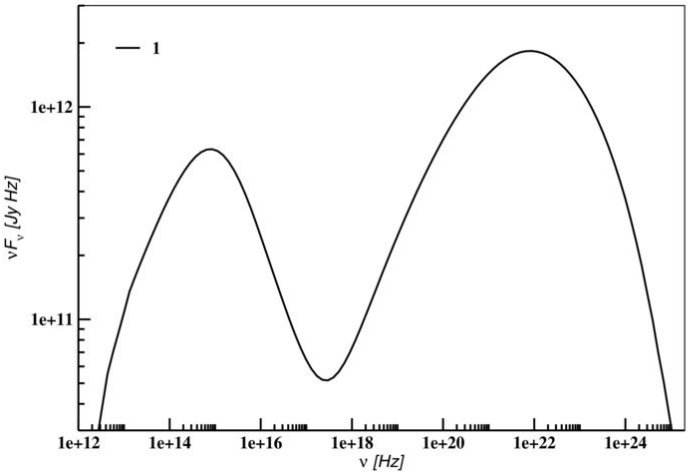

time-integrated SED

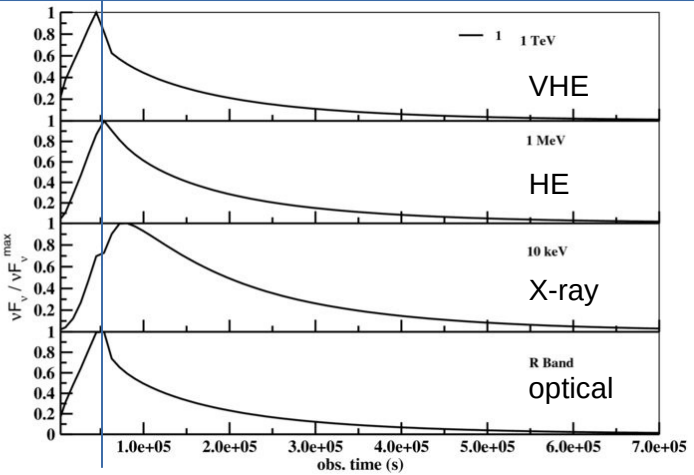

MWL light curves for a single collision.

optical flux : rise as long as the shocks are present in the emission region.
Then cooling dominates and the pulse begins to decline steadily.

HE photons : result of Compton up-scattering of optical photons off low-energy electrons → same peak as optical

X-ray flux : continues to rise even after the shocks exit the emission region → **peak delayed** and long asymmetric decay
- X-ray photons are produced from up-scattering of IR synchrotron photons off lower energy electrons, which cool slowly → slow intensity rise
- continued increase of late-arriving photons at the sites of scattering due to the **internal light crossing time effect.**

VHE photons : scattering of soft X-ray photons off higher-energy electrons that cool faster → **earlier peak than at optical / HE**

internal shocks

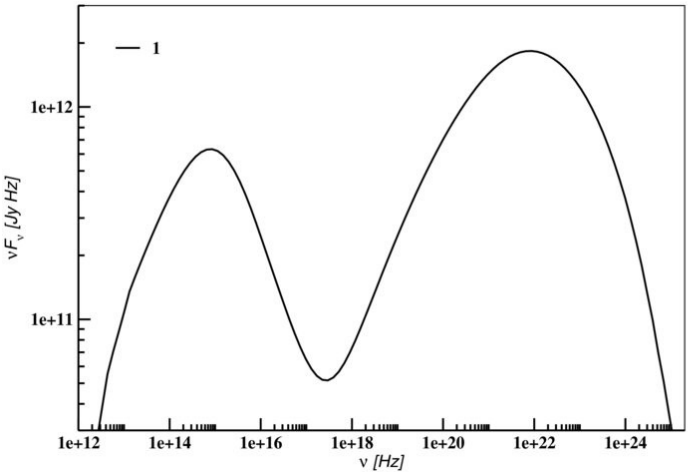

time-integrated SED

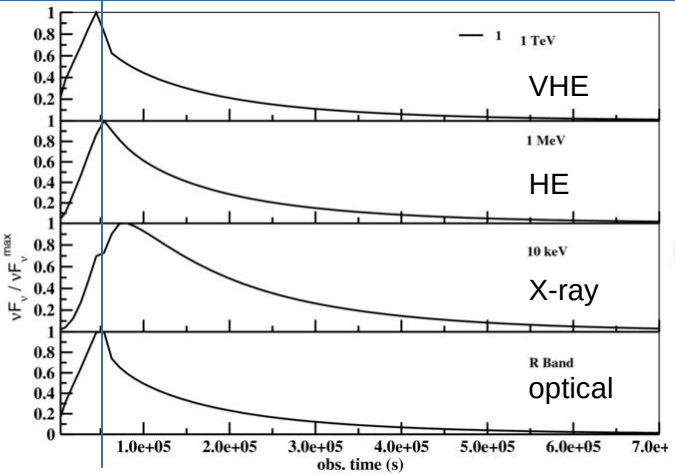

MWL light curves for a single collision.

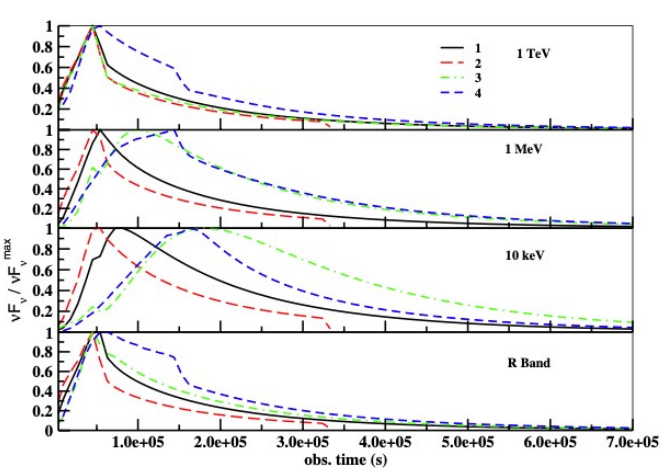

Effect of varying model parameters.

optical flux : rise as long as the shocks are present in the emission region.
Then cooling dominates and the pulse begins to decline steadily.

HE photons : result of Compton up-scattering of optical photons off low-energy electrons → same peak as optical

X-ray flux : continues to rise even after the shocks exit the emission region → **peak delayed** and long asymmetric decay
- X-ray photons are produced from up-scattering of IR synchrotron photons off lower energy electrons, which cool slowly → slow intensity rise
- continued increase of late-arriving photons at the sites of scattering due to the **internal light crossing time effect.**

VHE photons : scattering of soft X-ray photons off higher-energy electrons that cool faster → **earlier peak than at optical / HE**

turbulent plasma and standing shock

Turbulent, Extreme Multi-zone model (TEMZ)

- turbulent plasma flowing down a jet crosses a standing conical shock (e.g. recollimation shock).
- The shock compresses the plasma and accelerates electrons.
- Emission of **synchrotron** and **External Inverse Compton** on **IR photons from dust torus** and **photons from the Mach disk**.

- Turbulence is approximated as many cells, each with a uniform magnetic field with random direction.
- Density of high-energy electrons in the cells changes randomly with time following the power spectral density from observations.

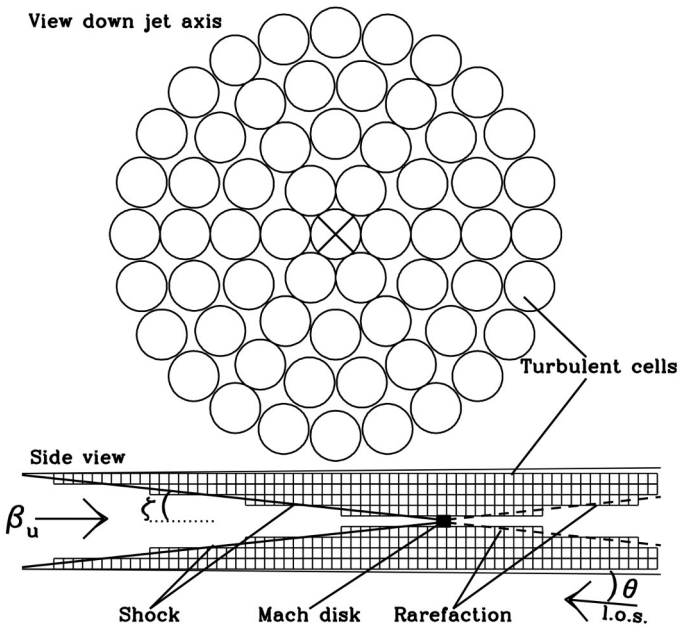

A.P. Marscher 2014 ++

turbulent plasma and standing shock

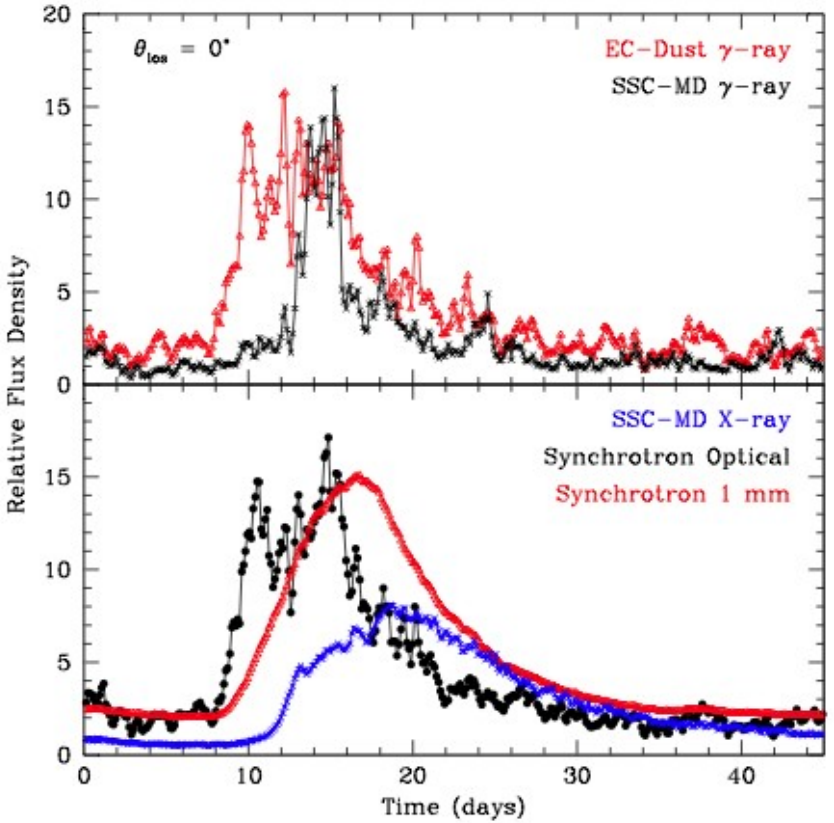

A.P. Marscher 2014

A test case using a rapid pulse of high density cells shows the generation of **time delays** :

Optical synchrotron & EC-Dust γ-rays :

Flux rises steeply as the pulse crosses the ring of computational cells at the upstream end of the shock.
Then it declines gradually as the pulse crosses smaller rings of cells.

Electrons that produce γ-ray and optical photons lose energy rapidly
→ radiation confined to a thin layer close to the shock.

turbulent plasma and standing shock

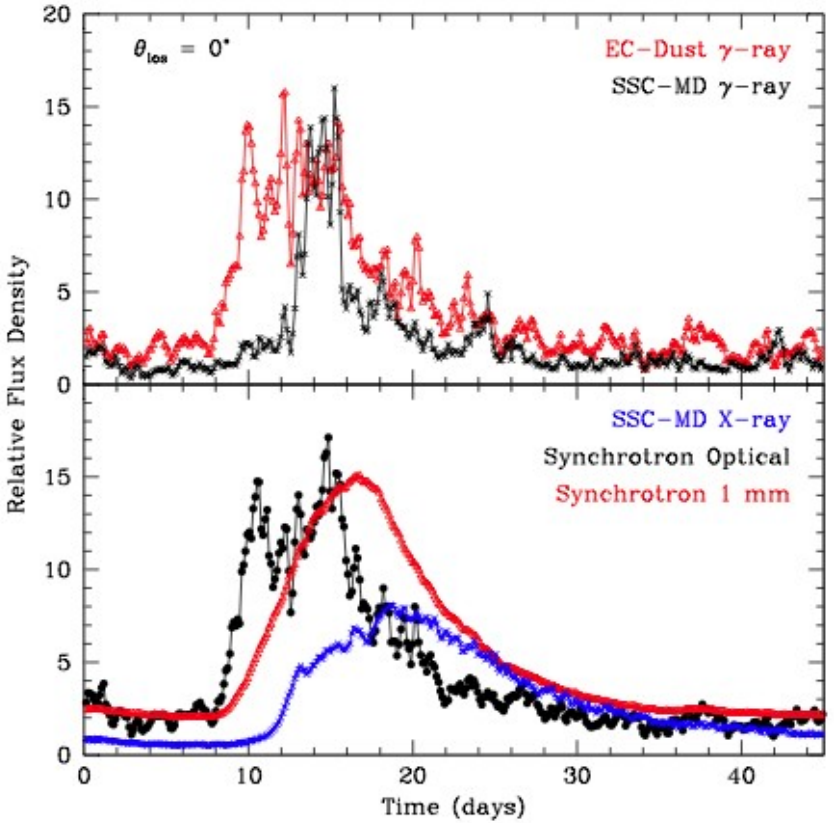

A.P. Marscher 2014

A test case using a rapid pulse of high density cells shows the generation of **time delays** :

Optical synchrotron & EC-Dust γ-rays :

Flux rises steeply as the pulse crosses the ring of computational cells at the upstream end of the shock.
Then it declines gradually as the pulse crosses smaller rings of cells.

Electrons that produce γ-ray and optical photons lose energy rapidly
→ radiation confined to a thin layer close to the shock.

Synchrotron 1 mm :

Electrons lose energy more slowly than for optical synchrotron
→ pulse delayed and slower decay

turbulent plasma and standing shock

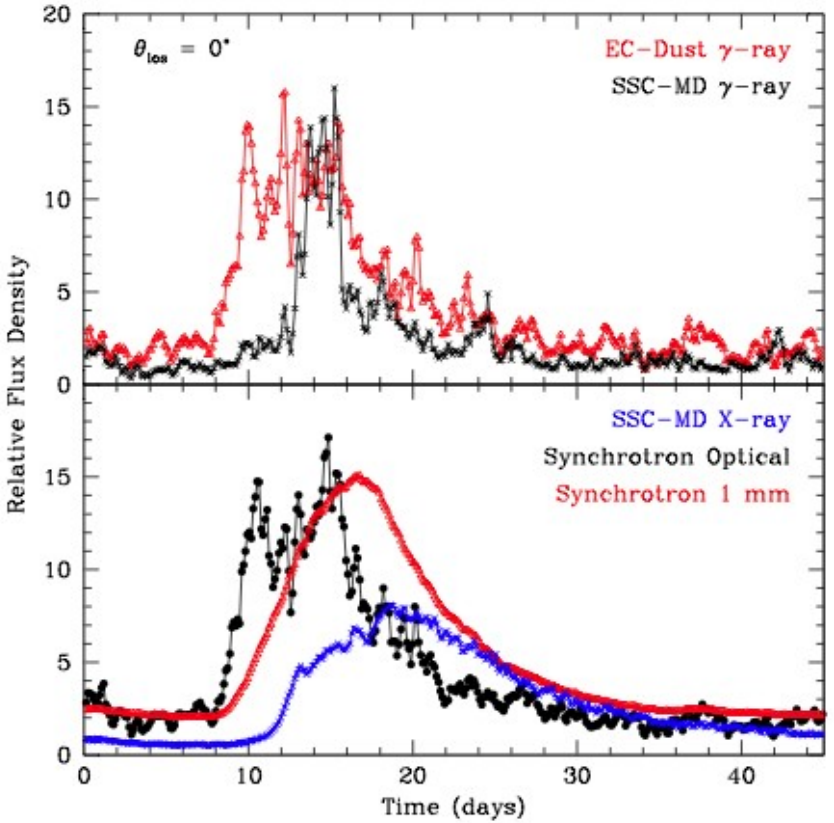

A.P. Marscher 2014

A test case using a rapid pulse of high density cells shows the generation of **time delays** :

Optical synchrotron & EC-Dust γ-rays :

Flux rises steeply as the pulse crosses the ring of computational cells at the upstream end of the shock.
Then it declines gradually as the pulse crosses smaller rings of cells.

Electrons that produce γ-ray and optical photons lose energy rapidly
→ radiation confined to a thin layer close to the shock.

Synchrotron 1 mm :

Electrons lose energy more slowly than for optical synchrotron
→ pulse delayed and slower decay

SSC-MD X-rays & **SSC-MD γ-rays** :

Flux increases modestly at first, then a rapid flare occurs as the pulse crosses the MD, creating a sudden increase in seed photon flux.

The X-ray pulse is longer due to slower cooling of the electrons.

magnetic reconnection zones

- reconnection events within the jet lead to particle acceleration and flares
  → requires high jet magnetization $\sigma \geq 1$ (↔ efficient shock acceleration requires low magnetization $\sigma \leq 10^{-2}$)

- simulation of plasmoids with PIC codes

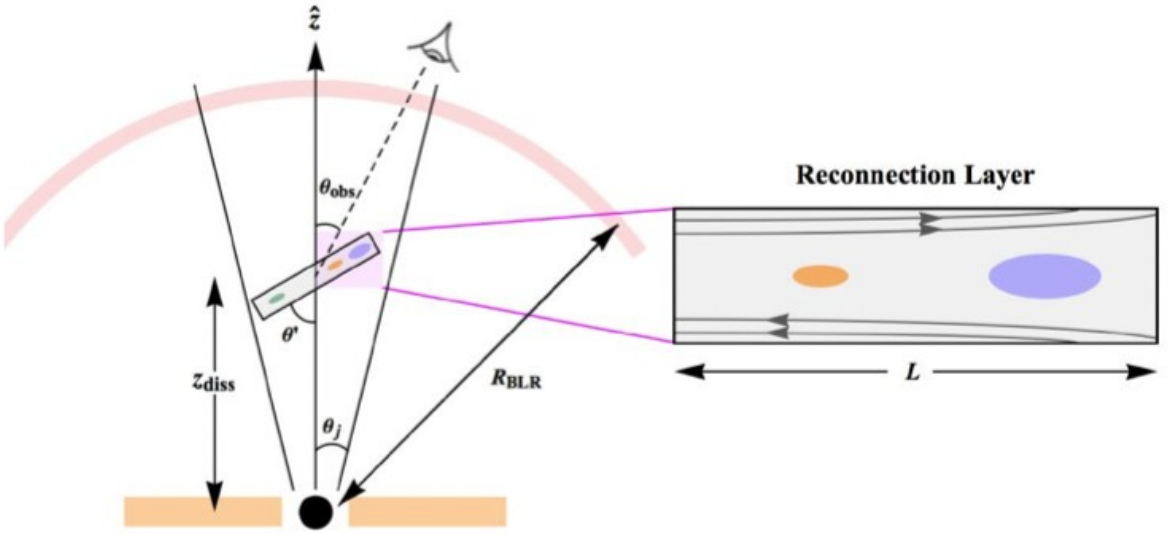

Petropoulou, Giannios, Sironi, 2016, MNRAS, 462, 3325
Sironi, Giannios, Petropoulou, 2016, MNRAS, 462, 48
Christie, Petropoulou, Sironi, Giannios, 2019, MNRAS, 482

magnetic reconnection zones

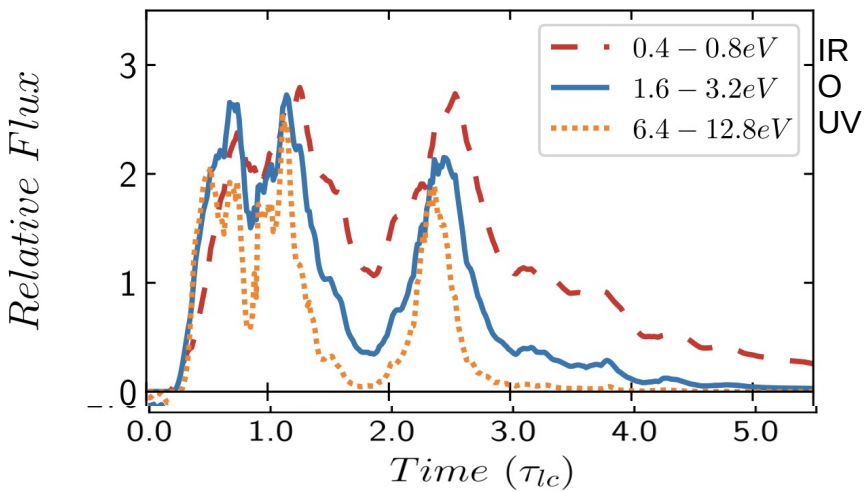

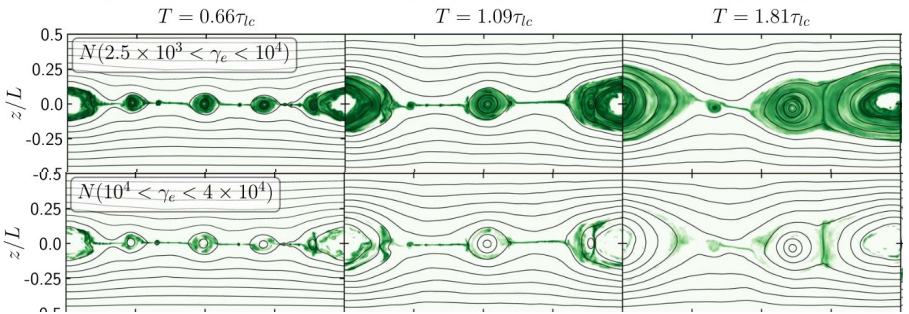

Study of light curves :

Higher-energy bands peak earlier than lower-energy bands.

The number of higher-energy particles peaks at the maximal efficiency of magnetic reconnection, i.e. in the **contact region** of two merging plasmoids, where the **acceleration is most efficient.**

As the merging moves **beyond the contact region**, **it can no longer accelerate these highest-energy particles**.

Additionally, synchrotron cooling is slower at lower energies, so electrons can continue to accumulate in the reconnection layer even if the reconnection efficiency drops.

H. Zhang, X. Li, D. Giannios et al. 2020

Conclusions

A variety of possible scenarios for the emergence of blazar flares,
depending on the location and physical conditions that characterize the acceleration / emission region.

(and more scenarios exist : emission from BH magnetosphere, cloud crossing jet ...)

More sophisticated modeling approaches ongoing : MHD + radiatif, PIC + radiatif ...

Conclusions

A variety of possible scenarios for the emergence of blazar flares,
depending on the location and physical conditions that characterize the acceleration / emission region.

(and more scenarios exist : emission from BH magnetosphere, cloud crossing jet ...)

More sophisticated modeling approaches ongoing : MHD + radiatif, PIC + radiatif ...

A variety of physical origins for energy-dependent delays :
- energy-dependent cooling and acceleration
- internal light-travel effects
- self-absorption (radio) and γγ-absorption (VHE)
- interplay between the emission of several regions that can dominate the observed flux
- interplay between different emission components (e.g. SSC, EIC on different fields)

Delays can go in both “directions”.

Conclusions

A variety of possible scenarios for the emergence of blazar flares,
depending on the location and physical conditions that characterize the acceleration / emission region.

(and more scenarios exist : emission from BH magnetosphere, cloud crossing jet ...)

More sophisticated modeling approaches ongoing : MHD + radiatif, PIC + radiatif ...

A variety of physical origins for energy-dependent delays :
- energy-dependent cooling and acceleration
- internal light-travel effects
- self-absorption (radio) and γγ-absorption (VHE)
- interplay between the emission of several regions that can dominate the observed flux
- interplay between different emission components (e.g. SSC, EIC on different fields)

Delays can go in both “directions”.

Better understanding of location and physical conditions of emission regions ?

→ well-sampled MWL datasets of rapid flares are still rare (especially for BL Lacs)

→ a variety of models exists, but comparison of different models against data is still the exception

backup

Outline

- Modeling approaches for blazar variability
- Single-zone models : particle injection / acceleration
- Single-zone models : propagation through photon fields
- Multi-zone models
- Conclusions

light-curves for different acceleration mechanisms

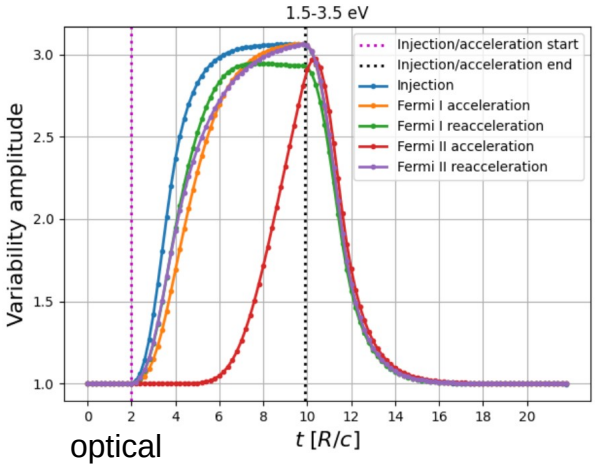

optical

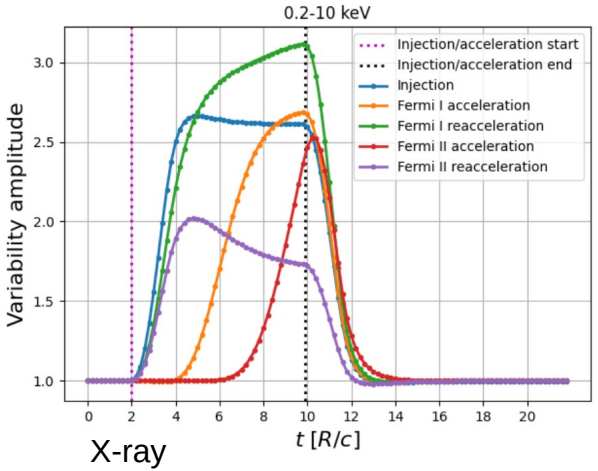

X-ray

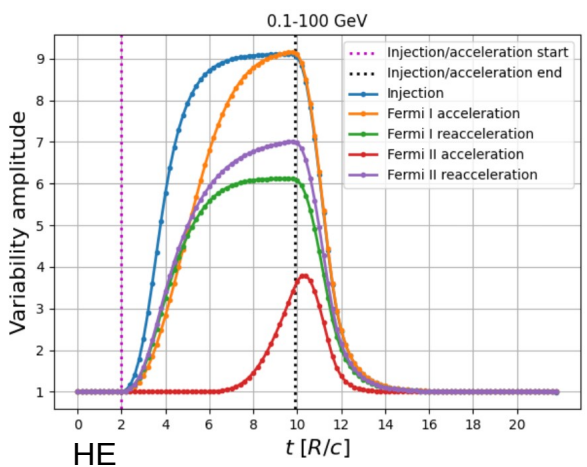

HE

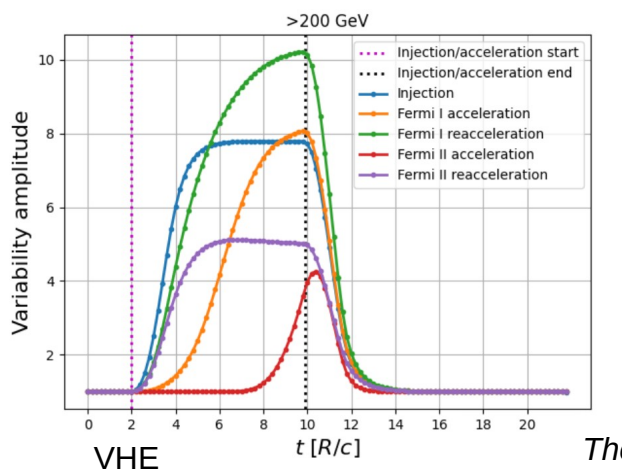

VHE

Time delays ?

Fermi I acceleration :

Delays between flare onset due to **gradual acceleration**.

Fermi II re-acceleration , Injection :

Flare peaks early in the X-ray band, then **IC cooling** sets in rapidly and leads to a flux decline.

Thevenet, AZ, Dmytriiev, Boisson, accepted A&A

accelerating blob model

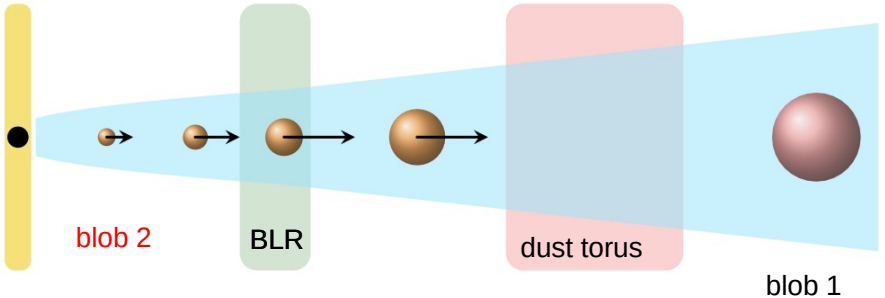

Le Bihan, Dmytriiev, AZ, 2025

low-state emission from a stationary emission region ("**blob 1**")

flare is caused by an accelerating, expanding emission region ("**blob 2**")

(differential collimation) :

$$\Gamma_{blob} = min\left(\Gamma_{max}, \sqrt{d/(3R_s)}\right)$$

(Ghisellini & Tavecchio 2009)

Γ_{max} = 30
→ acceleration up to ~ BLR

- for d < R_{BLR} , as blob 2 accelerates :

$$U' \propto d$$

- for d > d_{max}, as blob 2 advances at constant velocity :

$$U' \propto d^{-\beta_{BLR}}$$

- particle spectrum from injection of a steep power-law + cooling (incl. adiabatic) + particle escape

- B'_{blob1} = 0.09 G , initial B'_{blob2} = 0.03 G ,
  R'_{blob1} ~ 5 x 10^{16} cm, initial R'_{blob2} ~ 2 x 10^{15} cm

- relativistic effects important for BLR crossing
  Distance traveled in observed time interval Δt_{obs} :

$$D = \Delta t_{obs} \beta_{blob} c \delta \Gamma_{blob} / (1+z)$$

propagating blob model : hadronic vs. leptonic

A plasma blob is moving along the jet with constant velocity.

It is expanding following the constant jet opening angle.
B-field decreasing (magnetic flux is conserved)

Continuous injection of relativistic particles with constant power.

VHE band is fully absorbed at early times due to γγ pair production on photon fields → **delay** wrt other bands !

Effect of **pair production** (dashed lines) :

For large opening angles, t_{esc} becomes very large at large distance
→ **secondary flares** from pair production
→ more significant for hadronic scenario (secondary particles)

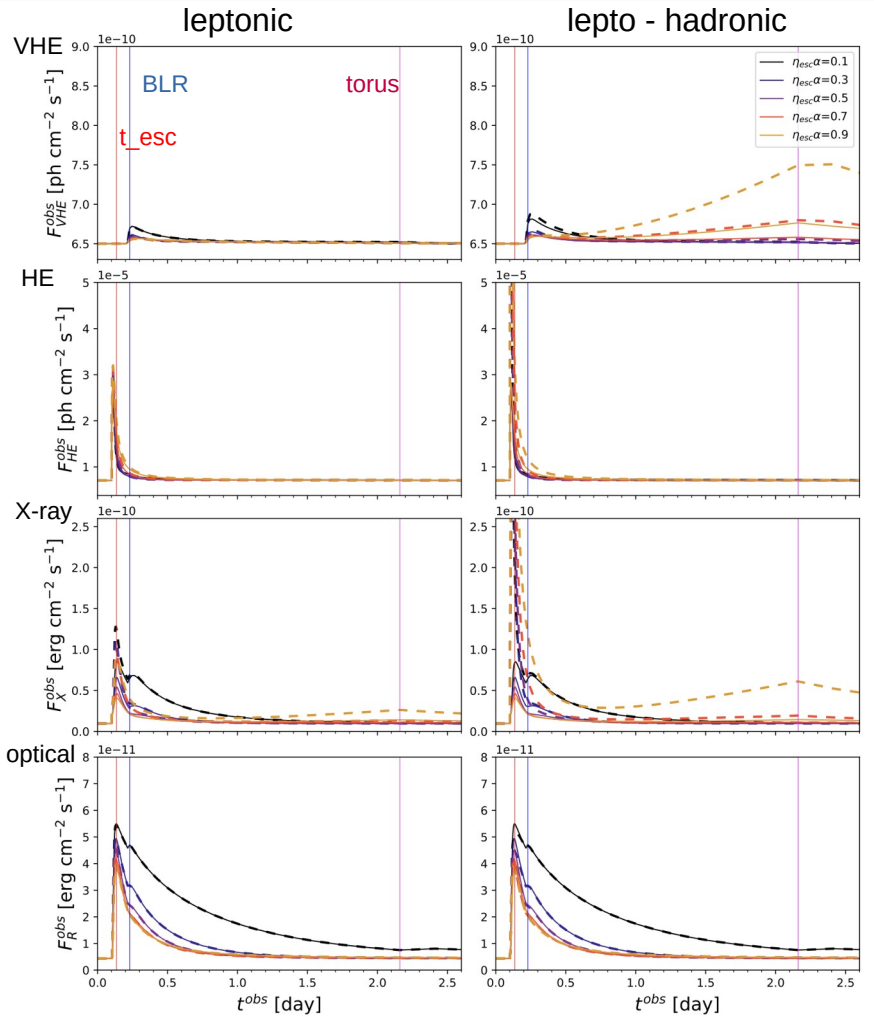

OneHaLe code
M. Zacharias 2023

jet/cloud interaction scenarios

very rapid variability seems possible if relativistic hadrons in the jet interact with stellar envelopes (red giants) or gas clouds (BLR) via p-p, p-γ or p-synchrotron.
(*e.g. D.V. Khangulyan, M.V. Barkov, V. Bosch-Ramon, F.A. Aharonian, A.V. Dorodnitsyn 2013*)

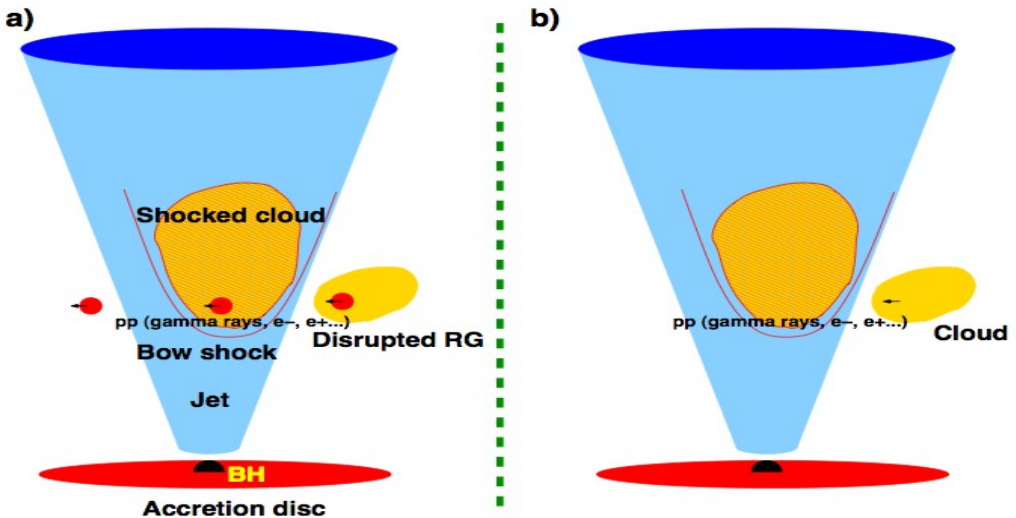

Bosch-Ramon, Perucho, Barkov, A&A (2012)

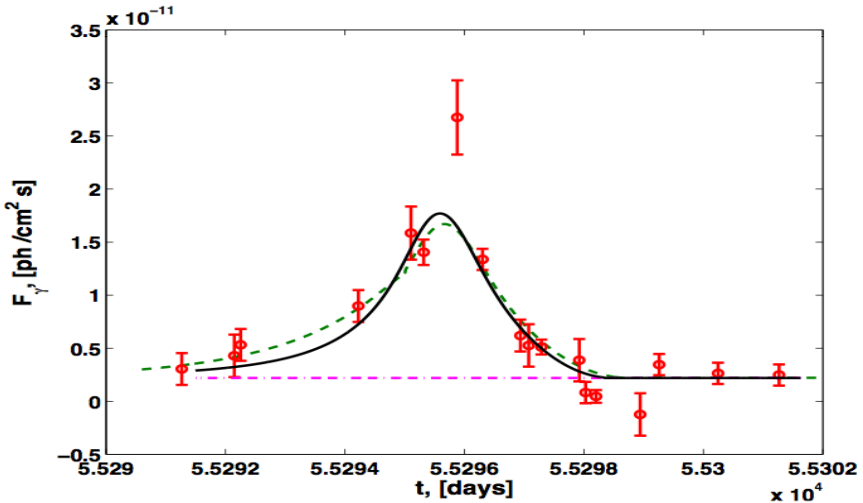

VHE flare of M87 in 2010

Barkov, Bosch-Ramon, Aharonian, ApJ (2012)

e.g. blazar flares in the Fermi-LAT band

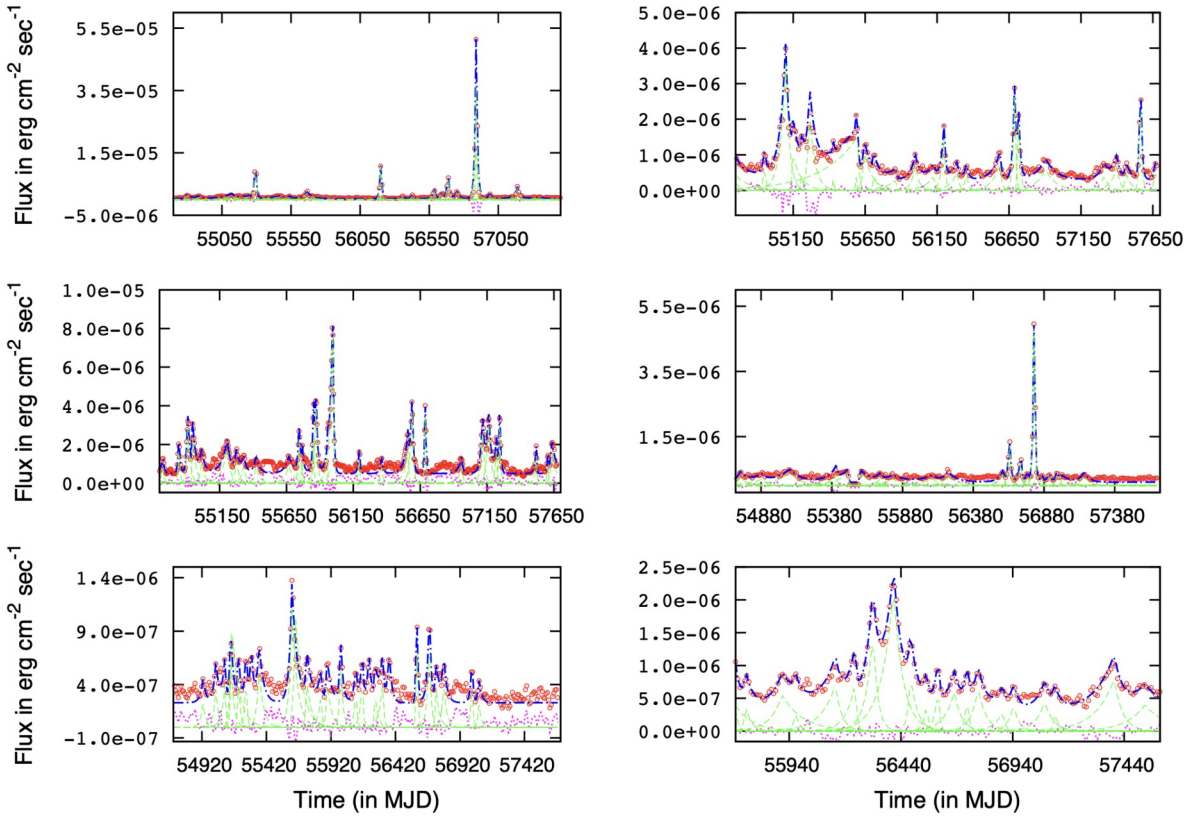

Figure 1. *Top left* – 3C 279; *top right* – 3C 273; *middle left* – 1510-089; *middle right* – Mrk 501; *bottom left* – PKS 2155-304; *bottom right* – PKS 1424-41. The red open circles denote the *Fermi*-LAT light curves of the above blazars at the energy range 0.1–300 GeV, which are smoothed with a Gaussian function of width 10 days; green long-dashed lines represent the individual decomposed flares (see the text), the blue dot–dashed line is the best fit to the model function given in Section 3.1, which is the sum of the individual flares, while the magenta dotted line is the residue after the fit.

Roy et al. 2019

For example *Roy et al. 2019* :

Study of long-term (~weeks–months) and short-term (~hour–day) GeV flares in a sample of 10 blazars from the Fermi-LAT and the Yale/SMARTS monitoring programme.

→ most long-term flares are symmetric : dominated by the crossing time-scale of a disturbance ?

→ larger fraction of short-term flares asymmetric : signature of gradual particle acceleration and cooling ?

rapid variability from the BH magnetosphere ?

Scenarios of pulsar-like particle acceleration by the electric field across a magnetospheric gap at the base of the radio jet.

- A maximally rotating BH with event horizon r_g accretes plasma. In the ergosphere extending to $2r_g$ in the equatorial plane, Poynting flux generated by frame-dragging effect (→ Blandford-Znajek)

- The rotation of the BH induces a magnetosphere with polar vacuum gap regions. In the gaps, the **electric field of the magnetosphere has a component parallel to the magnetic field** accelerating particles to ultra-relativistic energies.

- **Inverse-Compton scattering and pair production** due to interactions with low-energy thermal photons from the accretion disk leads to the observed gamma rays.

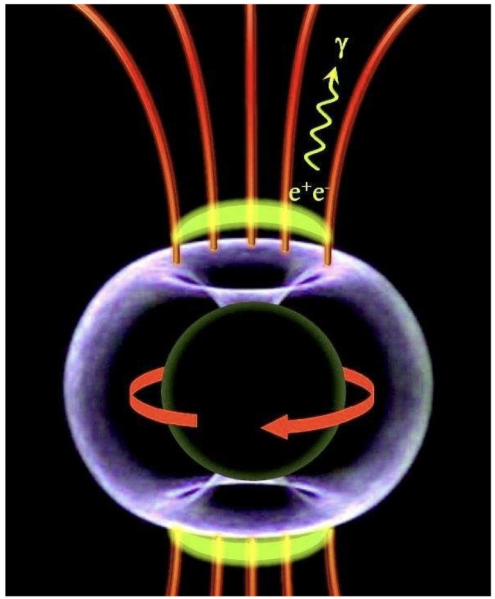

(Aleksic et al. 2014)

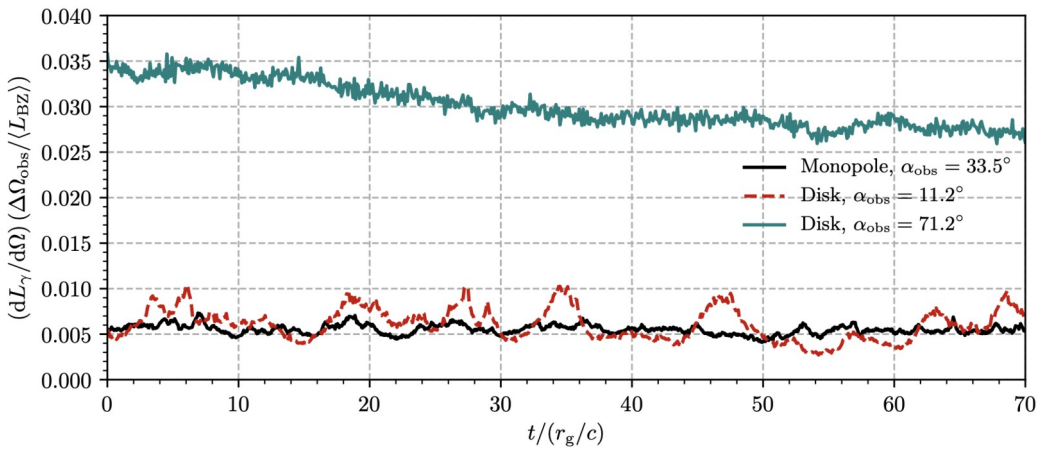

Add info

(Crinquand et al. 2021)

variation of the particle distribution

a systematic study

(P. Thevenet, AZ, C. Boisson, A. Dmytriiev;
submitted to A&A)

internal light-crossing effect

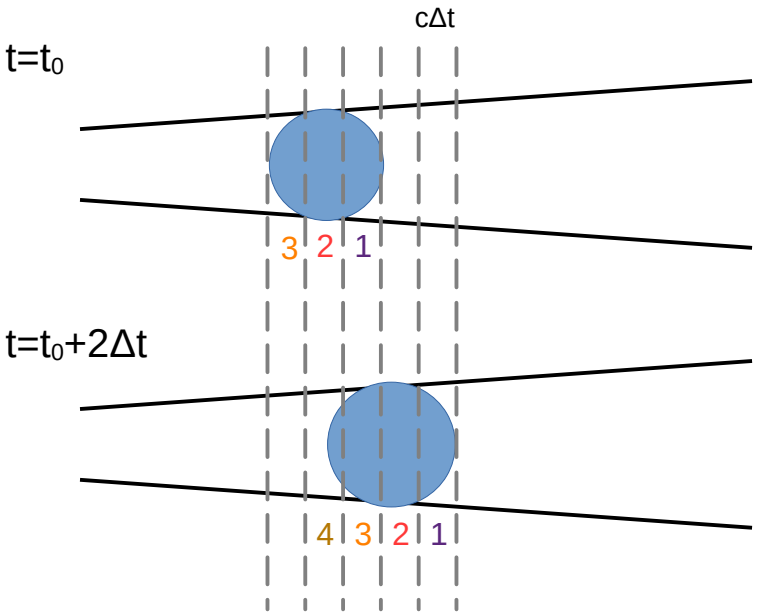

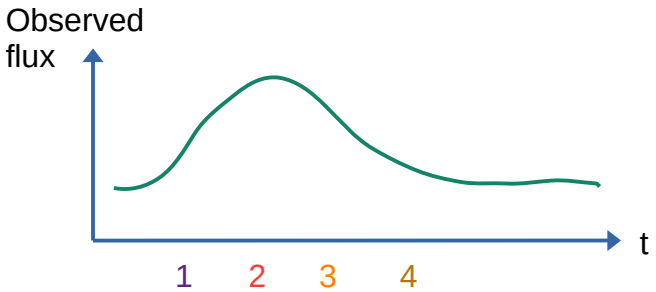

Correction for internal light-crossing effect
Inspired by the treatment in *jetset* (A.Tramacere).

→ “Smoothing” of simulated light curves.

the scenarios

injection

Q_{inj} : fixed injection rate, fixed PL spectrum, injected during flare window

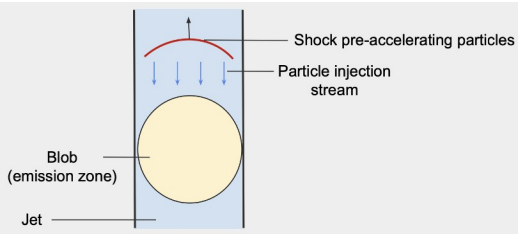

injection & adiabatic expansion

Q_{inj} plus fixed expansion rate

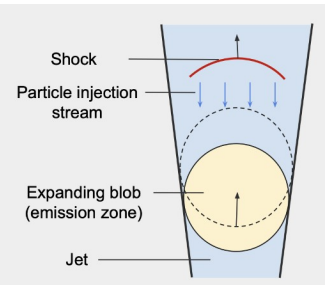

e.g. injection & adiabatic expansion

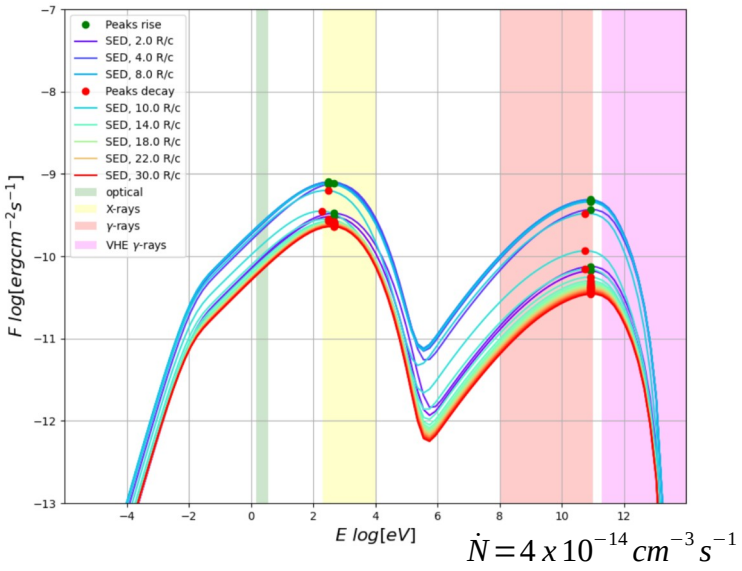

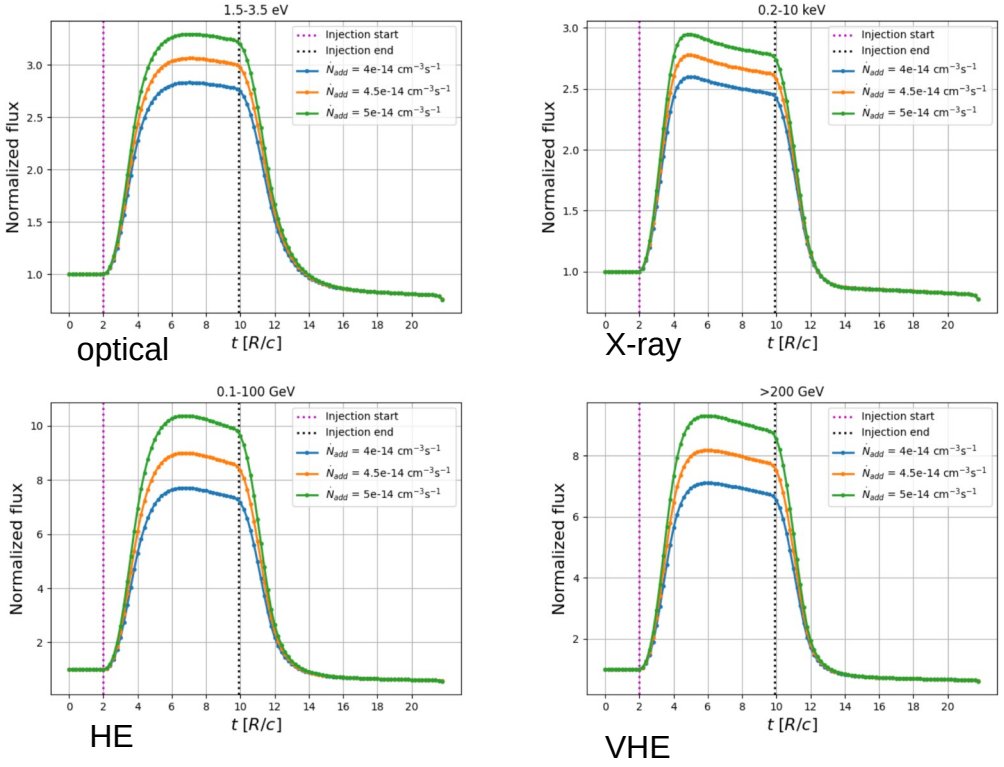

- shift of peaks during flare decay

- occurrence of a **plateau** (=high steady-state) in light curves

- flux decrease during plateau due to adiabatic expansion

the scenarios

injection

Q_{inj} : fixed injection rate, fixed PL spectrum, injected during flare window

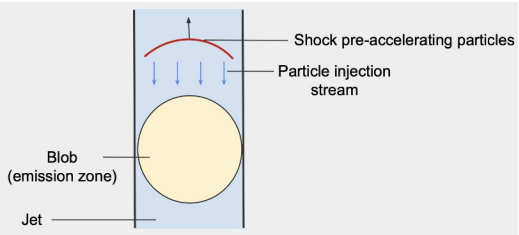

Fermi-I acceleration

Q_{inj} with increasing γ_{max} during flare window

t_{shock} : time-scale of γ_{max} evolution

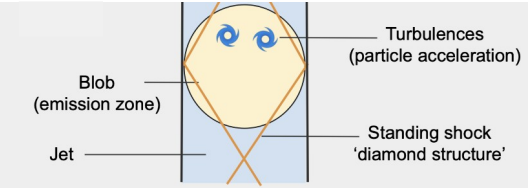

injection & adiabatic expansion

Q_{inj} plus fixed expansion rate

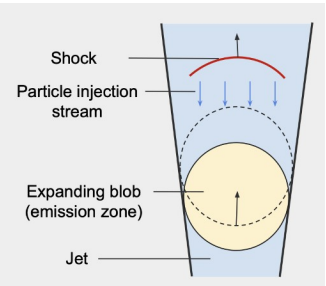

Fermi-I acceleration

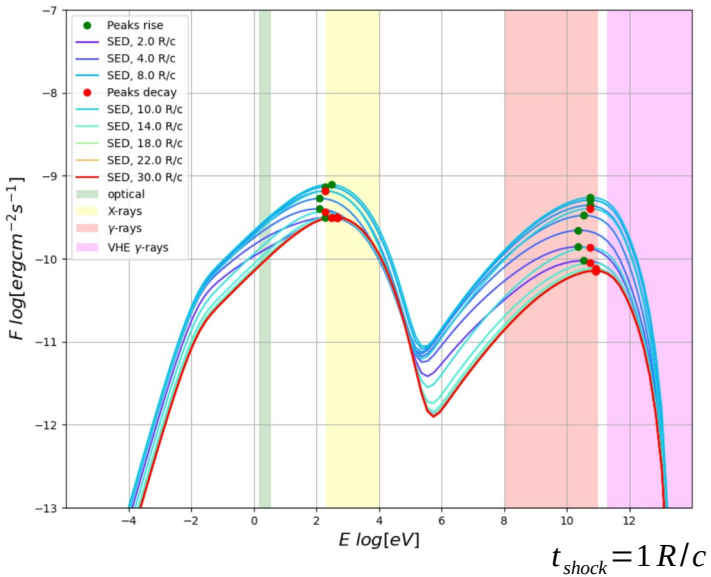

- shift of peaks during flare
  → clear **hysteresis**

- flare **onset** shifts between energy bands

- occurrence of a plateau only for very rapid t_{shock}

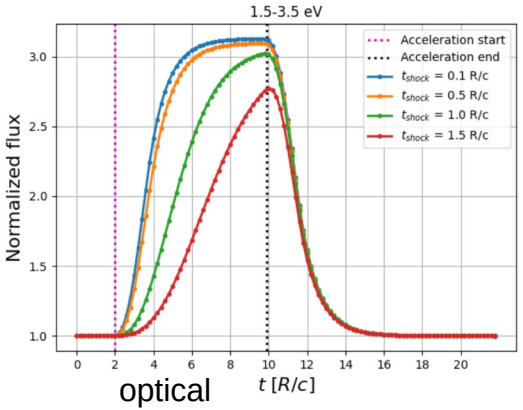

optical

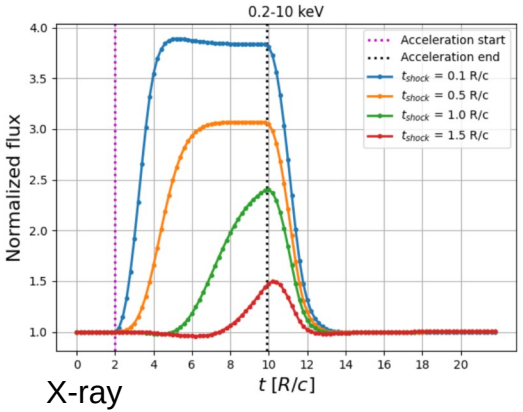

X-ray

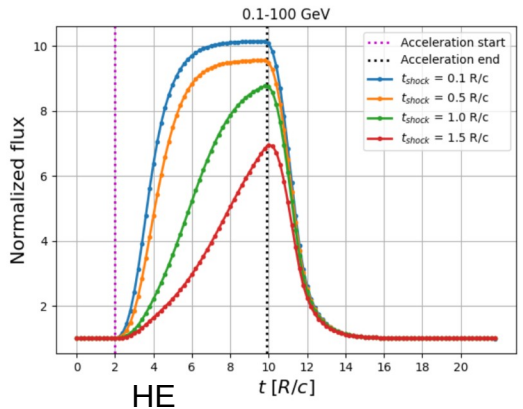

HE

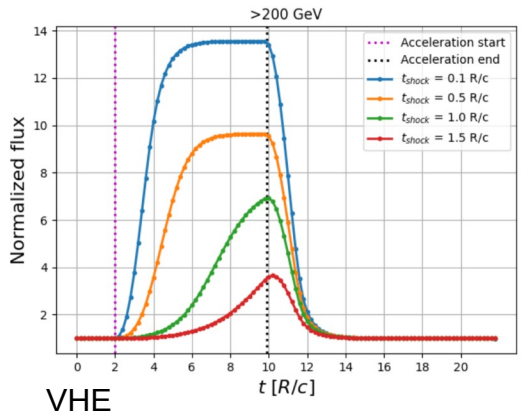

VHE

the scenarios

injection

Q_{inj} : fixed injection rate, fixed PL spectrum, injected during flare window

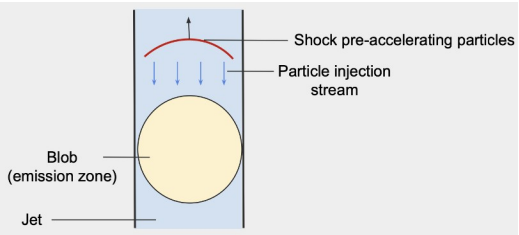

Fermi-I acceleration

Q_{inj} with increasing γ_{max} during flare window

t_{shock} : time-scale of γ_{max} evolution

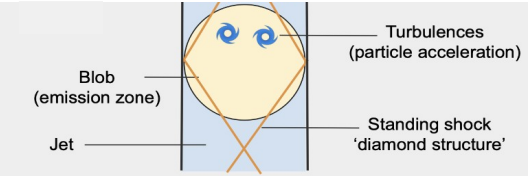

injection & adiabatic expansion

Q_{inj} plus fixed expansion rate

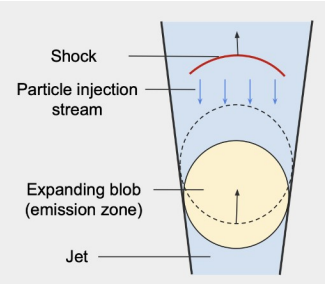

Fermi-I re-acceleration

Q_{inj} : fixed continuous PL injection

t_{FI} : time-scale for sys. energy gain

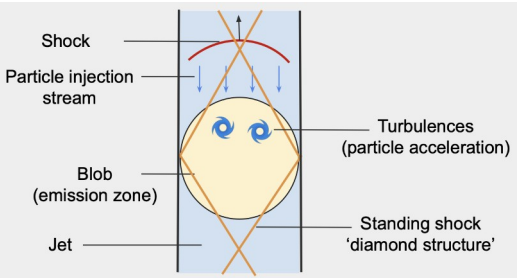

Fermi-I re-acceleration

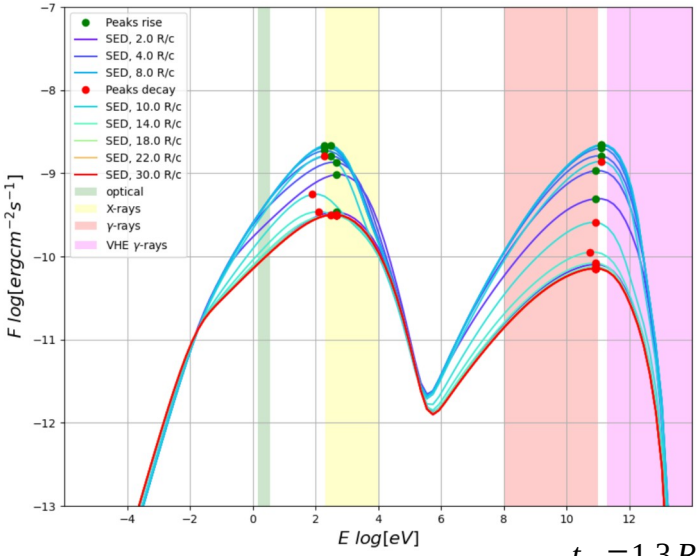

$t_{FI} = 1.3\,R/c$

- difference in flare shapes and peak times between optical/GeV and X-ray/TeV.

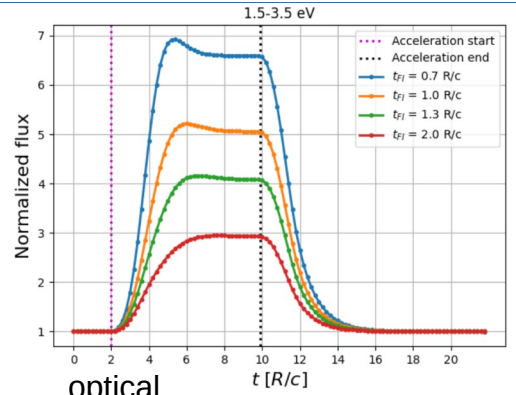

optical

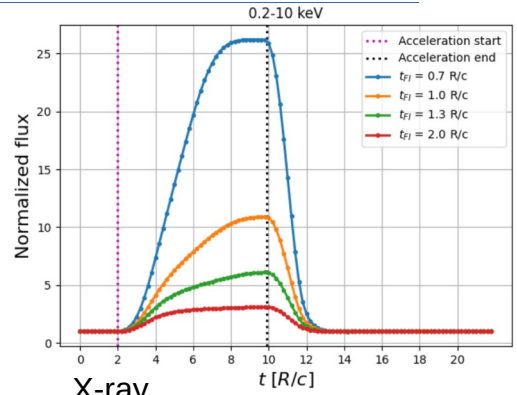

X-ray

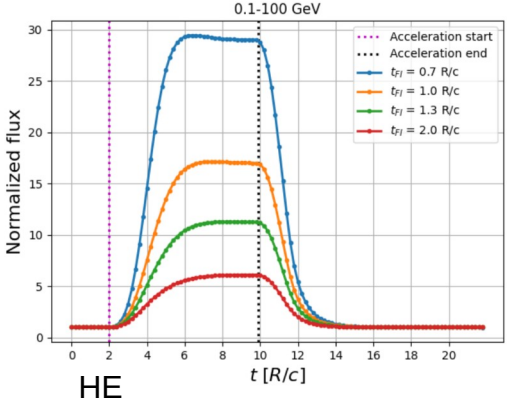

HE

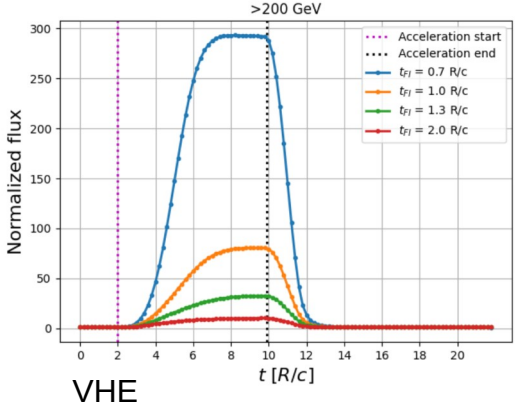

VHE

the scenarios

injection

Q_{inj} : fixed injection rate, fixed PL spectrum, injected during flare window

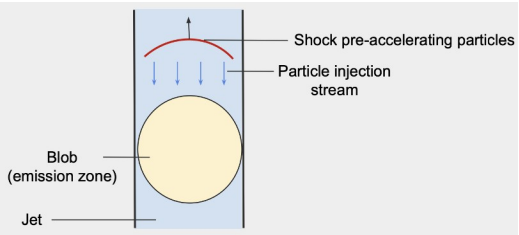

Fermi-I acceleration

Q_{inj} with increasing γ_{max} during flare window

t_{shock} : time-scale of γ_{max} evolution

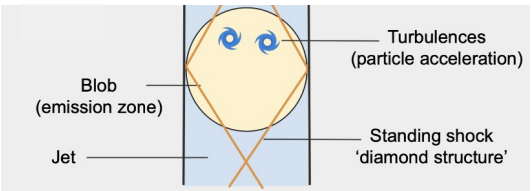

Fermi-II acceleration

injection of cold particles

t_{FII} : acceleration time scale

q=2 : hard-sphere scattering

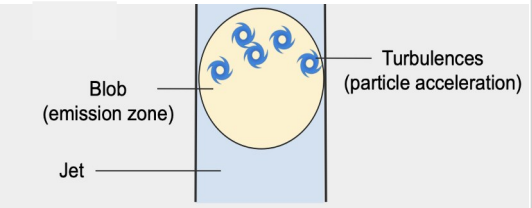

injection & adiabatic expansion

Q_{inj} plus fixed expansion rate

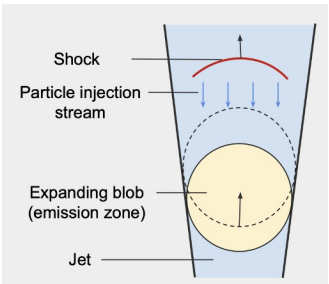

Fermi-I re-acceleration

Q_{inj} : fixed continuous PL injection

t_{FI} : time-scale for sys. energy gain

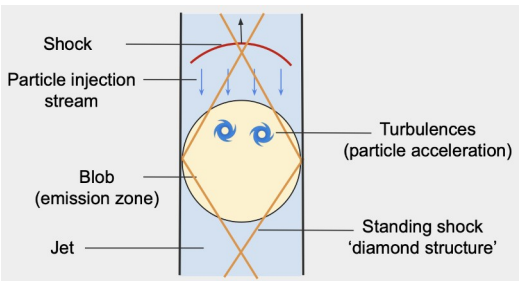

Fermi-II acceleration

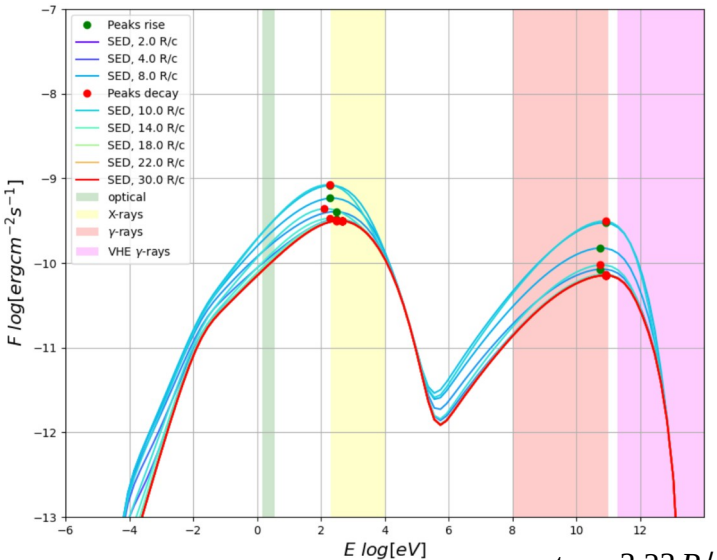

$t_{FII} = 3.23\, R/c$

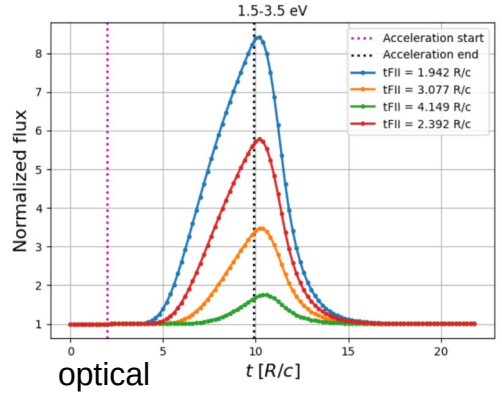

optical

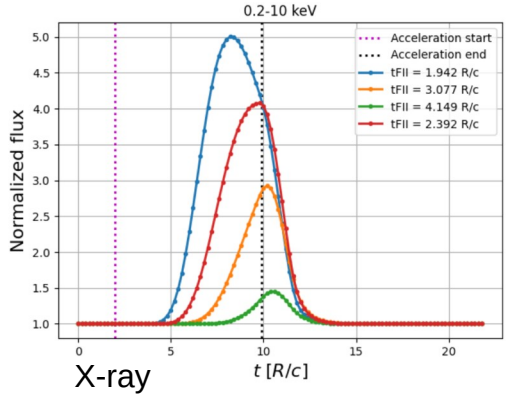

X-ray

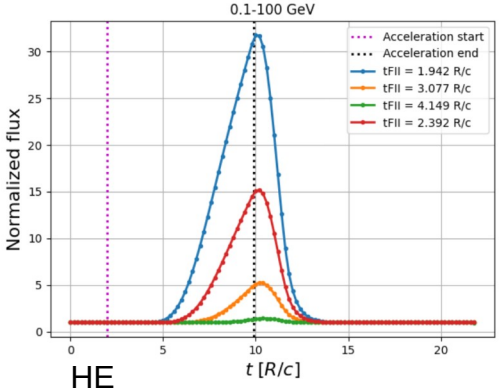

HE

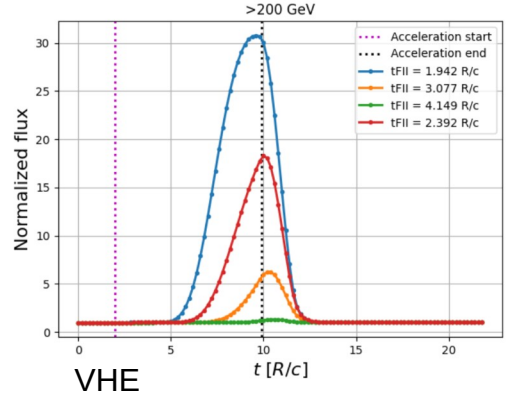

VHE

- **narrow** peaks without plateau

- X-ray light curve advances other bands for short t_{FII} due to rapid IC cooling.

the scenarios

injection

Q_{inj} : fixed injection rate, fixed PL spectrum, injected during flare window

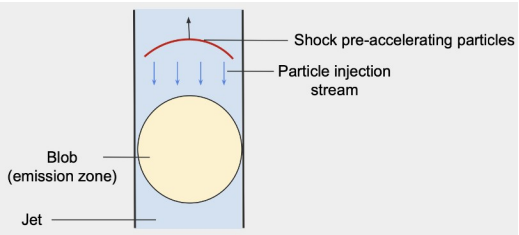

Fermi-I acceleration

Q_{inj} with increasing γ_{max} during flare window
t_{shock} : time-scale of γ_{max} evolution

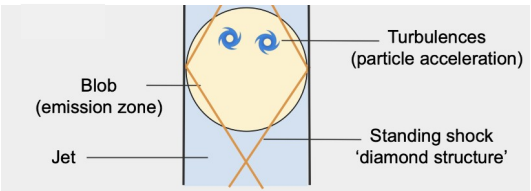

Fermi-II acceleration

injection of cold particles
t_{FII} : acceleration time scale
q=2 : hard-sphere scattering

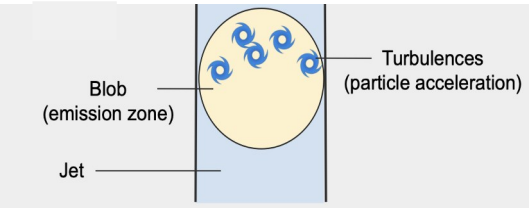

injection & adiabatic expansion

Q_{inj} plus fixed expansion rate

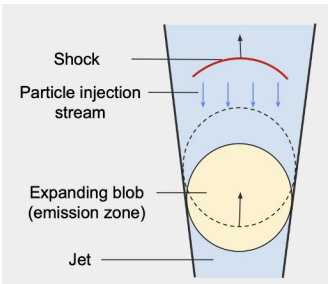

Fermi-I re-acceleration

Q_{inj} : fixed continuous PL injection
t_{FI} : time-scale for sys. energy gain

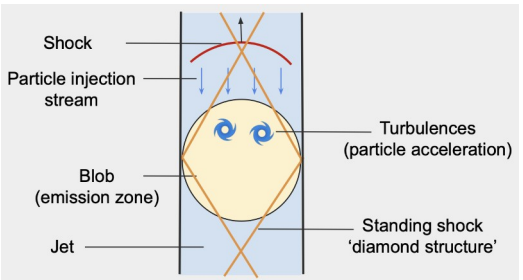

Fermi-II re-acceleration

Q_{inj} : fixed continuous PL injection
t_{FII} : acceleration time-scale , q=2

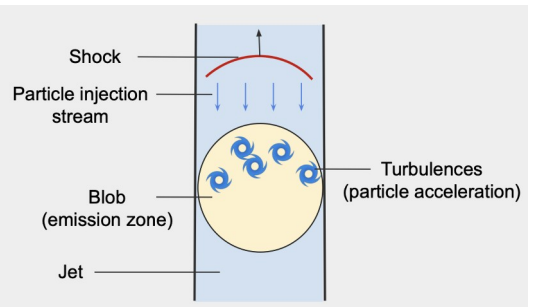

Fermi-II re-acceleration

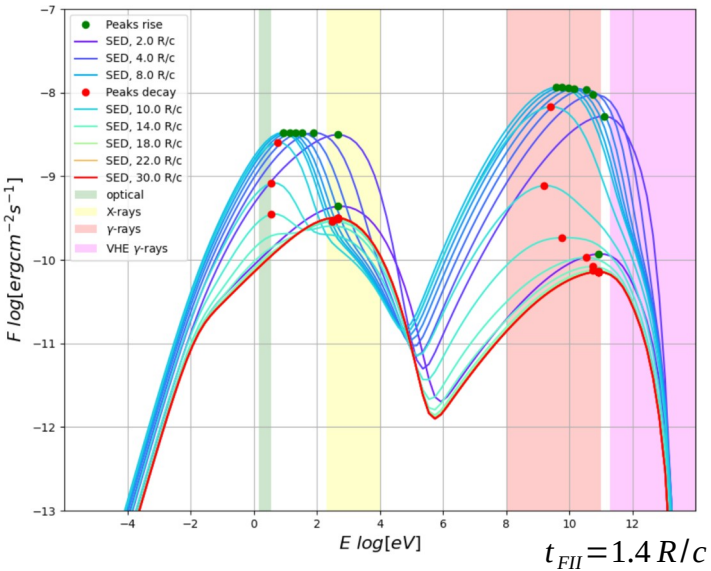

$t_{FII} = 1.4\,R/c$

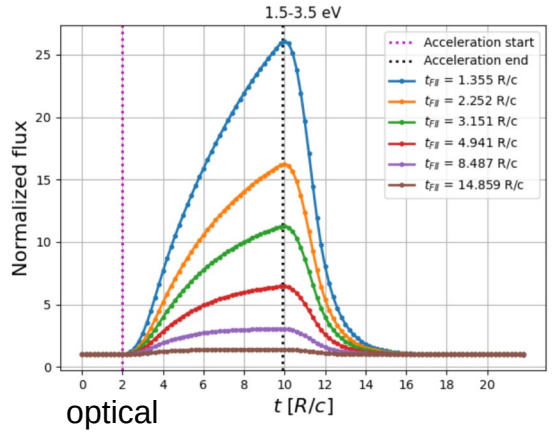

optical

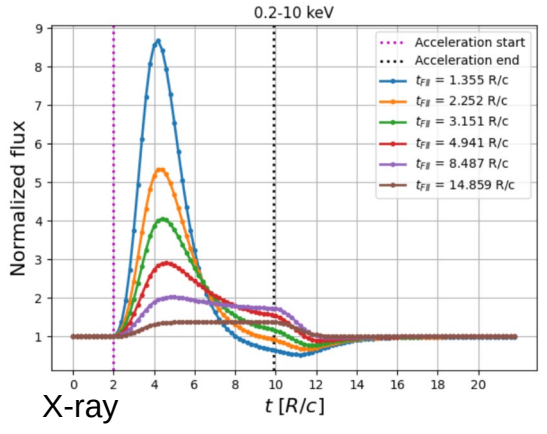

X-ray

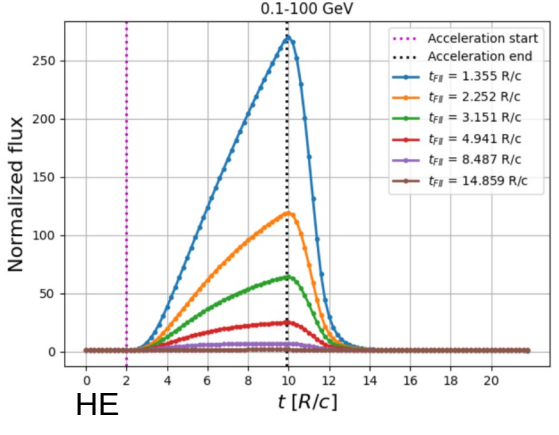

HE

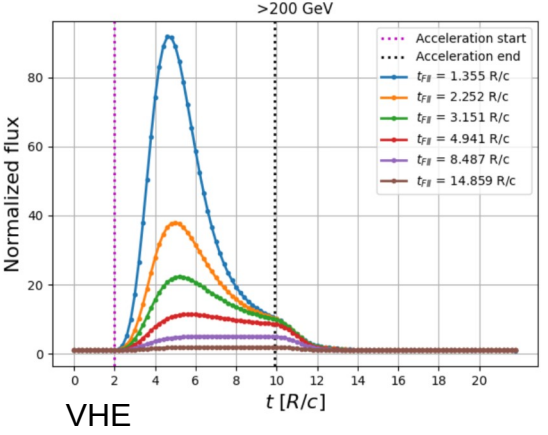

VHE

- strong shift of peaks during flare
  → **hysteresis**

- Compton dominance > 1 for very rapid t_{FII}

- strong energy dependent **time delays** between light curve peaks for very rapid t_{FII}

light-curve comparison

• **injection** scenarios :
Onset of the flare rise occurs at the same time in all bands.
Occurrence of plateaux.

• **Fermi-I** scenarios :
Flare onset is delayed at higher energies.

• **Fermi-II** scenarios :
Flare onset occurs ~ at the same time in different bands.
Acceleration of cold particles does not reach a plateau.
Efficient re-acceleration leads to a flare that is peaking earlier at higher energies.

Decay times determined by the escape time and the effect of radiative cooling.

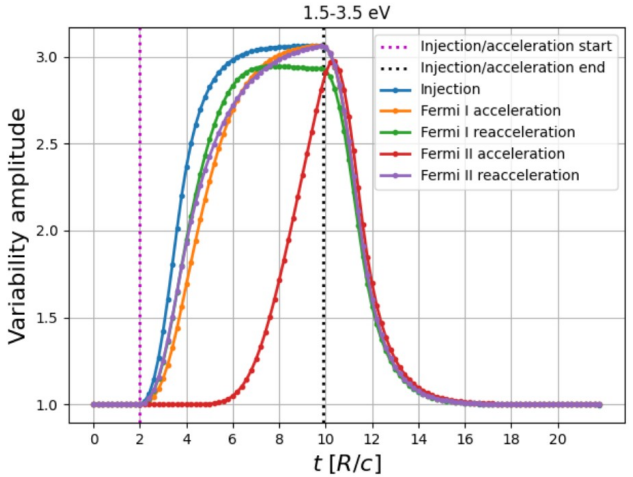

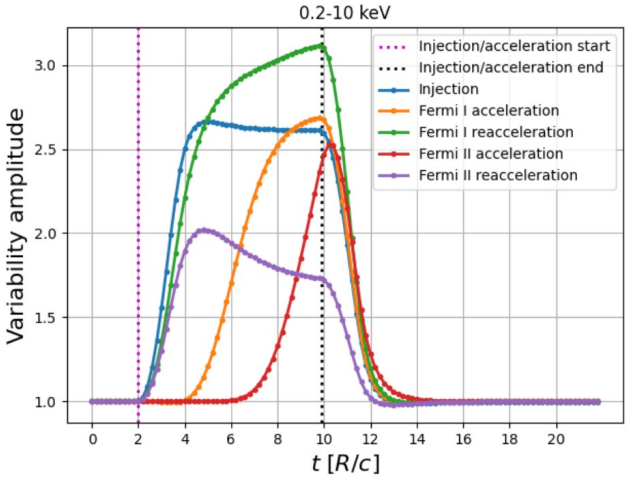

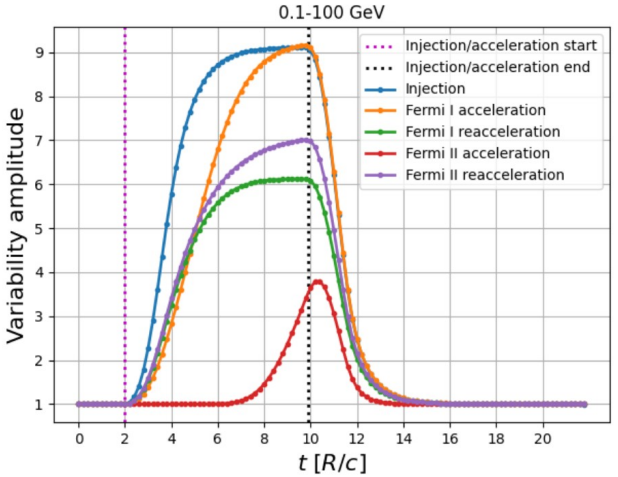

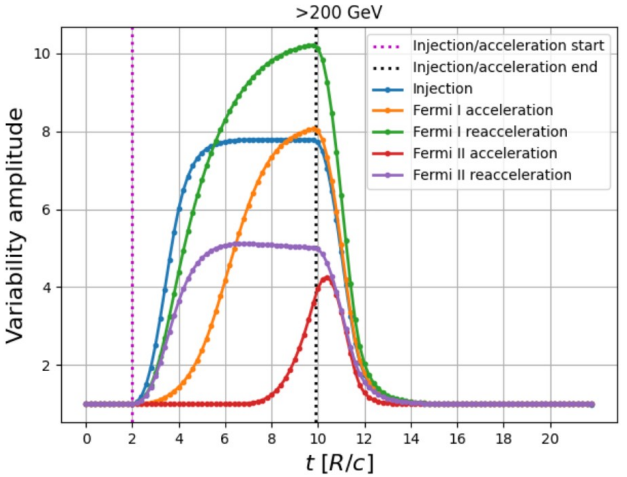

systematic study: parameter

Parameter	Variable	Value	Unit
Source			
Initial magnetic field	B_0	0.04	G
Magnetic field configuration	m_B	1	-
Initial blob radius	R_0	2.8×10^{16}	cm
Blob Doppler factor	δ	29	-
Redshift	z	0.0308	-
Angle to observer	θ	{0 ; 1}	°
Evolution			
Quiescent injection duration	$t_{\rm inj}$	30	R/c
Quiescent escape timescale	$t_{\rm esc}$	1	R/c
Beginning of expansion	$t_{\rm exp}$	0	R/c
Beginning of flaring	$t_{\rm flare}$	2	R/c
Duration of flaring	$t_{\rm dur}$	3	days (observer frame)
Escape timescale during flaring	$t_{\rm esc,flare}$	1	R/c
Continuous injection spectrum			
Spectrum normalization	$\dot{N}_{\rm inj}$	1.86×10^{-14}	$\rm cm^{-3}s^{-1}$
Spectrum slope	$\alpha_{\rm inj}$	-2.23	-
Pivot Lorentz factor	$\gamma_{\rm inj,pivot}$	1.0×10^5	-
Cutoff Lorentz factor	$\gamma_{\rm inj,cut}$	5.8×10^5	-
Minimal injected Lorentz factor	$\gamma_{\rm inj,min}$	800	-
Flaring injection spectrum			
Spectrum normalization	$\dot{N}_{\rm add}$	4×10^{-14}	$\rm cm^{-3}s^{-1}$
Spectrum slope	$\alpha_{\rm add}$	-2.23	-
Pivot Lorentz factor	$\gamma_{\rm add,pivot}$	1.0×10^5	-
Cutoff Lorentz factor	$\gamma_{\rm add,cut}$	5.8×10^5	-
Minimal injected Lorentz factor	$\gamma_{\rm add,min}$	800	-
Particle acceleration			
Fermi I re-acceleration timescale	$t_{\rm F_I}$	[0.7 – 2.0]	R/c
Turbulent spectrum slope	q	2	-
Maximum spectrum wavelength	$\lambda_{\rm max}$	[0 – 1]	R
Turbulence level	$\mathcal{L}_{\rm turb}$	[0 – 1]	-
Simulation grids			
Minimal electron Lorentz factor	$\gamma_{\rm min}$	100	-
Maximal electron Lorentz factor	$\gamma_{\rm max}$	1.0×10^7	-
Lorentz factor grid's points	n_γ	200	-
Simulation start time	$t_{\rm start}$	0	R/c
Simulation end time	$t_{\rm end}$	30	R/c
Time grid's bins	$n_{\rm bins}$	1000	-